Biphasic Internetwork Coordination is Funneled through an Electrical Synapse

Barathan Gnanabharathi
Savanna-Rae H Fahoum
Dawn M Blitz

Abbreviated Title: Biphasic Internetwork Coordination

Affiliations:
Department of Biology
Center for Neuroscience and Behavior
Miami University
Oxford OH 45056

Correspondence should be addressed to
Dawn M. Blitz
700 E High St
PSN 212
Oxford OH, 45056
blitzdm@miamoh.edu
513-529-6327

Acknowledgements: We thank Michael Hughes and Anh Vo (Statistical Consulting Center, Miami University) for assistance with statistical analysis.

Conflict of Interest:
The authors report no conflict of interest.

Funding sources: National Science Foundation IOS:1755283 (DMB), Biology Department, Miami University

Abstract

Linked rhythmic behaviors, such as respiration/locomotion or swallowing/chewing often require coordination for proper function. Despite its prevalence, the cellular mechanisms controlling coordination of the underlying neural networks remain undetermined in most systems. We use the stomatogastric nervous system of the crab *Cancer borealis* to investigate mechanisms of internetwork coordination, due to its small, well characterized feeding-related networks (gastric mill [chewing, ~0.1 Hz]; pyloric [filtering food, ~1 Hz]). Here, we investigate coordination between these networks during the Gly^1-SIFamide (SIF) neuropeptide modulatory state. SIF activates a unique triphasic gastric mill rhythm in which the typically pyloric-only LPG neuron generates dual pyloric- plus gastric mill-timed oscillations. Additionally, the pyloric rhythm exhibits increased cycle frequency during gastric mill rhythm-timed LPG bursts, and decreased cycle frequency during IC, or IC plus LG gastric mill neuron bursts. Hyperpolarizing current injections and photoinactivation of network neurons demonstrate that gastric mill rhythm bursts in IC, but not LG, are responsible for decreasing the pyloric frequency, whereas LPG increases pyloric frequency through its rectified electrical coupling to pyloric pacemaker neurons. Surprisingly, LPG photoinactivation also eliminated slowing of the pyloric rhythm. IC firing frequency and gastric mill burst duration were not altered by LPG photoinactivation, suggesting that IC slows the pyloric rhythm primarily via synaptic inhibition of LPG, which then slows the pyloric pacemakers via electrical coupling. Thus, despite its rectification, an electrical synapse directly conveys endogenous bursting and indirectly funnels neurotransmitter-mediated inhibition to enable one network to alternately increase and decrease the frequency of a related network.

Significance Statement

Related rhythmic behaviors frequently exhibit coordination, yet the cellular mechanisms coordinating the underlying neural networks are not determined in most systems. We investigated coordination between two small, well-characterized crustacean feeding-associated networks during a neuropeptide-elicited modulatory state. We find that a dual fast/slow network neuron directly increases fast network frequency during its slow, intrinsically generated bursts, via electrical coupling to fast network pacemakers, despite rectification favoring the opposite direction. Additionally, the fast network is indirectly slowed during another slow-network phase, via chemical synaptic inhibition funneled through the same electrical synapse. Thus, a rectifying electrical synapse alternately reinforces and diminishes neuropeptide actions, enabling distinct frequencies of a faster network across different phases of a related slower rhythm.

Introduction

Many rhythmic behaviors require coordination for proper function, such as locomotion and respiration, and multiple orofacial behaviors (e.g., respiration, swallowing, chewing, whisking, vocalization) (Barnett et al., 2021; Cao et al., 2012; Hao et al., 2021; Huff et al., 2022; Juvin et al., 2022; Wei et al., 2022). Central pattern generator (CPG) networks controlling rhythmic behaviors are flexible to accommodate changing organismal needs (Bucher et al., 2015; Grillner and El Manira, 2020; Ramirez and Baertsch, 2018). Behavioral coordination requires coordinating the underlying CPG networks. Significant consequences occur from disrupted coordination, such as aspiration of food if swallowing and respiration are not coordinated (Yagi et al., 2017). Thus, it is important to understand the cellular-level mechanisms controlling internetwork coordination.

Coordination can occur in multiple forms. Networks may express correlated changes in frequency or strength, as occurs in respiration to meet the demands of changing locomotor speeds, or at the onset of vocalizations (Anderson et al., 2016; Demartsev et al., 2022; Juvin et al., 2022; Ramirez and Baertsch, 2018). Coordination may also involve relative timing relationships, such as specific delays between movements of different body parts, or a regulated number of cycles of one behavior relative to another (Daley et al., 2013; Juvin et al., 2022; Mulloney and Smarandache-Wellmann, 2012; Wei et al., 2022). Such interactions may occur via direct CPG to CPG projections, or indirectly via feedback from networks to higher-order inputs to a related CPG, for example (Bartos and Nusbaum, 1997; Gariépy et al., 2010; Wood et al., 2004). Additional anatomical substrates to coordinate network activity include sensory

160 feedback from one behavior influencing related CPGs, or parallel descending input to
161 related networks (Barnett et al., 2021; Gariépy et al., 2010; Juvin et al., 2022). More
162 complex behavioral interactions may also occur, such as nesting of the mouse crying
163 rhythm nested within respiration, or dynamic changes in respiration during singing in
164 mice, birds, or humans, or while playing wind instruments (Fortune et al., 2011; Hérent
165 et al., 2023; Higashino et al., 2022; Okobi et al., 2019; Wei et al., 2022). Further,
166 coordination can be altered by developmental, physiological, or environmental stimuli
167 (Blitz and Nusbaum, 2008; Clemens et al., 1998a; Moore et al., 2013; Saunders et al.,
168 2004; Sillar et al., 2023; Stein and Harzsch, 2021). Although insights have been gained
169 into internetwork coordination, its complexity and plasticity coupled, with often large,
170 distributed networks make it difficult to fully determine how network coordination is
171 controlled (Juvin et al., 2022).

172 Here we used small, well-described networks in the stomatogastric nervous
173 system (STNS) of the Jonah crab, *Cancer borealis*, to investigate cellular-level
174 mechanisms of internetwork coordination (Bartos et al., 1999; Bartos and Nusbaum,
175 1997; Daur et al., 2016; Wood et al., 2004). An in vitro STNS preparation includes the
176 stomatogastric ganglion (STG, ~30 neurons) containing well-characterized CPGs that
177 control the gastric mill (food chewing) and pyloric (food filtering) rhythms, plus identified
178 modulatory and sensory inputs (Fig. 1) (Blitz, 2023; Daur et al., 2016; Nusbaum and
179 Beenhakker, 2002). The pacemaker-driven pyloric rhythm is constitutively active (~1
180 Hz), whereas the slower (~0.1 Hz) network-driven gastric mill CPG requires activation
181 by modulatory or sensory inputs (Blitz, 2023; Nusbaum and Beenhakker, 2002).
182 Although the gastric mill and pyloric rhythms can occur independently, they are often

183 coordinated, and the extent and type of coordination is altered by modulatory,
184 behavioral, and environmental conditions (Bartos et al., 1999; Bartos and Nusbaum,
185 1997; Blitz et al., 2019; Clemens et al., 1998a; Stein and Harzsch, 2021; Wood et al.,
186 2004).

187 We investigated mechanisms of coordination during the modulatory state elicited
188 by the modulatory commissural neuron 5 (MCN5), or bath application of its
189 neuropeptide Gly^1-SIFamide (Blitz et al., 2019; Fahoum and Blitz, 2024, 2021). In this
190 state, the typically pyloric-only LPG switches into dual pyloric and gastric mill rhythm
191 participation, becoming the third phase of a gastric mill rhythm (Fahoum and Blitz,
192 2024). This contrasts with biphasic gastric mill rhythm versions (Beenhakker et al.,
193 2004; Blitz et al., 2008, 1999; Christie et al., 2004). The pyloric rhythm frequency varies
194 across the Gly^1-SIFamide gastric mill rhythm, but a full description plus identification of
195 mechanisms of interactions between the two networks is lacking (Blitz et al., 2019). The
196 well-described connectome and small populations (1-5 neurons/neuron type) enabled
197 selective manipulation of neuronal populations to determine the full extent of gastric mill
198 regulation of the pyloric rhythm and its underlying cellular mechanisms during the
199 unique triphasic Gly^1-SIFamide-elicited gastric mill rhythm. Our results highlight the
200 complexity of synaptic connectivity that can mediate coordination between related
201 networks.

202

203 **Methods**

204 **Animals**

205 Wild caught adult male *C. borealis* crabs were procured from The Fresh Lobster
206 Company (Gloucester, MA), maintained in artificial seawater (10-12°C) tanks, and fed
207 twice weekly until used. Prior to dissection, crabs were anesthetized by cold packing in
208 ice for 40 – 50 minutes. The crab foregut was first removed, bisected, and pinned flat,
209 ventral side up, in a Sylgard 170-lined dish (Thermo Fisher Scientific). The STNS was
210 then dissected free from muscles and connective tissue and pinned in a Sylgard 184-
211 lined petri dish (Thermo Fisher Scientific) (Fahoum and Blitz, 2021; Gutierrez and
212 Grashow, 2009). The preparation was kept in chilled (4°C) *C. borealis* physiological
213 saline throughout dissections.

214

215 **Solutions**

216 *C. borealis* physiological saline was composed of 440 mM NaCl, 26 mM $MgCl_2$,
217 13 mM $CaCl_2$, 11 mM KCl, 10 mM Trizma base, 5 mM maleic acid (pH 7.4-7.6). Squid
218 internal electrode solution contained 10 mM $MgCl_2$, 400 mM potassium D-gluconic acid,
219 10 mM HEPES, 15 mM Na_2SO_4, 20 mM NaCl, pH 7.45 (Hooper et al., 2015). Gly^1-
220 SIFamide (GYRKPPFNG-SIFamide, custom peptide synthesis: Genscript) (Blitz et al.,
221 2019; Dickinson et al., 2008; Huybrechts et al., 2003; Yasuda et al., 2004) was
222 prepared by dissolving it in optima water (Thermo Fisher Scientific) at 10 mM, and
223 aliquoting and storing it at -20°C. Aliquots were diluted in physiological saline to a final
224 concentration of 5 μM before use in experiments.

225 **Electrophysiology**

226 The STNS preparation was superfused continuously with chilled *C. borealis*
227 physiological saline (8 - 10°C), or Gly[1]-SIFamide (5 μM) diluted in saline. A switching
228 manifold enabled uninterrupted superfusion of the STNS preparation during solution
229 changes. Extracellular activity was recorded from nerves with custom stainless-steel pin
230 electrodes and a model 1700 A-M Systems Amplifier. The stomatogastric ganglion
231 (STG) was desheathed to gain access for intracellular recording of STG somata. Light
232 transmitted through a dark field condenser (MBL-12010 Nikon Instruments) provided
233 visualization of STG neuron somata. For intracellular recordings of STG neurons, sharp-
234 tipped glass microelectrodes pulled using a glass electrode puller (P-97, Flaming/Brown
235 microelectrode puller, Sutter Instrument Co.) were used. Microelectrodes were filled
236 with a squid internal solution (see Solutions) (resistance: 20 – 40 MΩ) (Hooper et al.,
237 2015). Axoclamp 900A amplifiers (Molecular Devices) were used to collect intracellular
238 recordings in current clamp mode. Recordings were collected before, during, and after
239 the transection of both inferior and superior oesophageal nerves (*ion* and *son,*
240 respectively), to isolate the STG from descending neuromodulatory inputs. Data
241 presented were collected after transections were performed, unless otherwise noted.
242 For intracellular recordings, STG neuronal cell bodies were identified using extracellular
243 nerve recordings and/or their interactions with other STG neurons. All recordings were
244 collected using acquisition hardware (Micro1401; Cambridge Electronic Design) and
245 software (Spike2 Version 8.02e; ~5kHz sampling rate; Cambridge Electronic Design)
246 and a laboratory computer (Dell).

247 A data set from Fahoum and Blitz (2021) was re-used in this study for analysis of
248 a different set of parameters from the previous study. As described, activity in the
249 inferior cardiac (IC), lateral gastric (LG), or dorsal gastric (DG) neurons, or all three
250 neurons simultaneously, was eliminated via hyperpolarizing current injection (-2 to -4
251 nA). Neurons were hyperpolarized sufficiently to eliminate spike-mediated and graded
252 transmitter release (Fahoum and Blitz, 2021).

253 For the established biological model of MCN5 actions, for all experiments using
254 bath-application of Gly^1-SIFamide (5 μM), the lateral pyloric (LP) neuron was either
255 hyperpolarized (-2 to -4 nA) or photoinactivated (Fahoum and Blitz, 2021; Snyder and
256 Blitz, 2022). To selectively eliminate the influence of the single LP neuron or the two
257 copies of the LPG neurons, neurons were impaled with a microelectrode that was tip-
258 filled with AlexaFluor-568 hydrazide (10 mM in 200 mM KCl; Thermo Fisher Scientific)
259 and backfilled with squid internal solution. The neurons were injected with -5 nA
260 hyperpolarizing current (for either ~ 30 min, or for 5 to 10 min and the dye then allowed
261 to diffuse for an additional ~30 min) to fill their soma and neurites with the AlexaFluor-
262 568 dye. The STG was then illuminated with a Texas red filter set (560 ± 40 nm
263 wavelength; Leica Microsystems, 3-7 min). The neurons were considered completely
264 photoinactivated when the membrane potential reached 0 mV, and their action
265 potentials were absent in either the lateral ventricle nerve (*lvn;* for LP) or the lateral
266 posterior gastric nerve (*lpgn;* for LPG).

267

268

Data analysis

Neuronal Activity Parameters

The number of bursts, burst duration (s), cycle period (s; start of one burst to the start of the subsequent burst of a reference neuron), number of spikes per burst, and firing frequency (Hz; [number of spikes per burst – 1]/burst duration) were quantified using a custom Spike2 script. Each activity parameter was averaged across 20 min, unless otherwise noted. All analyses were performed after the effects of Gly^1-SIFamide application reached steady state. Steady state was noted when LPG elicited consistent dual-network bursting (e.g., Fig. 1Ciii) with consistent gastric mill-timed bursting of LG, IC, and DG (~ 10 min from the start of Gly^1-SIFamide bath application). The pyloric cycle period was quantified as the duration(s) from the start of one pyloric dilator (PD) neuron burst to the start of the subsequent PD burst (Bartos et al., 1999). In the Saline:*ions*/*sons* cut condition, in which the *ions/sons* where transected, the pyloric cycle period did not always express a full triphasic pattern, due to the lack of modulatory input (Hamood et al., 2015; Spencer and Blitz, 2016; Zhang et al., 2009). However, when this occurred, the pyloric rhythm returned during the Gly^1-SIFamide bath application. A Saline:*ions/sons* cut condition was excluded from analysis if PD neuron bursting was intermittently active, was completely absent, or if the PD neurons were rhythmically active but had ≤ 2 action potentials per burst. Pyloric cycle periods were measured across the final 20 min of 30 min Gly^1-SIFamide (5 μM) bath applications, and across 200 s windows for Saline:Intact STNS and the Saline:*ion/son* cut conditions.

Gastric mill-timed IC bursts were identified as those that had burst durations greater than 0.45 s (Blitz et al., 2019; Fahoum and Blitz, 2024). Multiple IC bursts with

292 greater than 0.45 s burst durations, were grouped into a single “gastric mill” burst if the
293 distance between each burst was less than 2 s, otherwise they were considered as
294 individual bursts. If there was an IC burst with a burst duration less than 0.45 s between
295 two gastric mill IC bursts that were less than 2 s apart, they were grouped together as
296 one gastric mill burst. Within an IC gastric mill-timed burst, pyloric-timed IC bursts were
297 identified if there was an interruption timed to a PD burst (e.g., Fig. 6Ai-ii). We identified
298 LPG gastric mill-timed bursts (LPG slow bursts) as previously described (Fahoum and
299 Blitz, 2024, 2021; Snyder and Blitz, 2022). Briefly, from a histogram of all LPG inter-
300 spike intervals (ISIs) made in Excel (Microsoft), peaks of intraburst (interval between
301 spikes during a burst) and interburst (interval between spikes between burst) intervals
302 were identified. The mean ISI was calculated between these two peaks and used to
303 identify LPG bursts. A custom written Spike2 script was then used to identify LPG
304 gastric mill-timed slow bursts and exclude pyloric-timed LPG bursts using PD activity as
305 a reference (Fahoum and Blitz, 2021). Coefficient of variation (CV) of pyloric cycle
306 periods was calculated as Standard Deviation / Mean.
307

308 **Analysis of pyloric cycle period relative to gastric mill neuron activity**

309 To analyze pyloric cycle periods based on which gastric mill neurons were active,
310 burst timings for each neuron over a 20 min window, unless otherwise indicated, were
311 exported from Spike2 to MATLAB (MathWorks) for further analysis. A custom written
312 MATLAB script categorized PD cycle periods according to which gastric mill neuron(s)
313 bursts overlapped with each pyloric cycle. This included any amount of overlap between
314 a pyloric cycle period and a gastric mill neuron burst. Pyloric cycle periods that did not

overlap with any gastric mill neurons were placed into the SIFbaseline category, i.e., no gastric mill neurons active. The average pyloric cycle period within each category was averaged across experiments. For some categories there were no cycle periods in a particular experiment. Specifically, in the data set of 19 preparations, there were cycle periods assigned to the IC, LPG:IC, and LPG:DG:IC categories in 9-10 preparations, while there were cycle periods assigned to the remaining 13 categories in 16-19 preparations. This data set (n=16/19 from Fahoum and Blitz, 2021) and the LPG:Intact and LPG:Kill condition experiments (n=9/9 from Fahoum and Blitz, 2024) were reanalyzed from previous studies. Two experiments from the original data set of 11 were excluded from analysis due to a lack of biphasic regulation in the LPG:Intact condition.

Due to the inter-preparation variability of the pyloric cycle period, to test for changes in regulation of the pyloric cycle period between LPG:Kill and LPG:Intact conditions, all pyloric cycle periods were normalized to the average pyloric cycle period in the SIFbaseline category in each experiment. All pyloric cycle periods after normalization were plotted as a histogram with a bin size of 3 ms for both conditions. Further, bin counts for each histogram were normalized to the peak count in that condition to compare the overall distribution of the two histograms. Normalization and histogram plotting were performed using a custom written MATLAB script.

Figure preparation and statistical analysis

Burst and spike identification from raw data was performed with custom-written scripts in Spike2, and exported to either Microsoft Excel or MATLAB for further analysis.

338 Pyloric cycle period histograms were plotted using a script written in MATLAB. Figures
339 were created using graphs and recordings exported from MATLAB, SigmaPlot (Systat,
340 v13), and Spike2 into CorelDraw (Corel, v24). Statistical analyses were performed using
341 SigmaPlot software and R statistical software (v4.1.1). Data were analyzed for normality
342 using the Shapiro-Wilk test to determine whether a non-parametric or parametric test
343 would be used. Paired *t* test, One Way Repeated Measures ANOVA, mixed model
344 ANOVA, and *post hoc tests* were used as noted. For all tests, we used an alpha level of
345 0.05. Data are presented as mean ± SE.

346

347 **Code accessibility**

348 Spike2 and MATLAB scripts used for analysis are available at
349 https://github.com/blitzdm/GnanabharathiFahoumBlitz2024.

350

351 **Results**

352 **Gly^1-SIFamide elicits a variable pyloric rhythm**

353 The modulatory projection neuron MCN5 elicits a unique gastric mill rhythm that
354 can be reproduced in vitro by bath application of the MCN5 neuropeptide Gly^1-SIFamide
355 plus elimination of LP neuron activity (Blitz et al., 2019; Fahoum and Blitz, 2024, 2021).
356 All pyloric and gastric mill neurons are identified, occur with a small copy number (1-5
357 neurons/type) and the connectivity mapped under multiple modulatory conditions (Fig.
358 1B) (Daur et al., 2016; Marder and Bucher, 2007). In *C. borealis*, LPG is typically only
359 active with the pyloric network due to its electrical coupling with the rest of the pyloric

360 pacemaker ensemble (Fig. 1B-C) (Shruti et al., 2014), but switches into dual-network
361 activity characterized by longer slower gastric mill-timed bursts (slow bursts) alternating
362 with shorter duration, faster pyloric-timed bursts during Gly^1-SIFamide application (Fig.
363 1Ciii) (Blitz et al., 2019; Fahoum and Blitz, 2024, 2021). The unique Gly^1-SIFamide
364 gastric mill rhythm is characterized by co-activity of LG and IC neurons that are primarily
365 out of phase with DG neuron activity, followed by LPG neuron gastric mill activity (Blitz
366 et al., 2019; Fahoum and Blitz, 2024) (Fig. 1C). Anecdotally, the pyloric rhythm
367 frequency varies throughout the Gly^1-SIFamide gastric mill rhythm, with a correlation
368 between IC burst duration and extended duration pyloric cycles (Blitz et al., 2019;
369 Fahoum and Blitz, 2021). Here we investigate in detail the relationship between pyloric
370 rhythm frequency and the gastric mill rhythm in the Gly^1-SIFamide modulatory state.

371 We first quantified the variability of the pyloric rhythm by measuring the
372 coefficient of variation (CV) in control and during the Gly^1-SIFamide gastric mill rhythm.
373 To eliminate confounds due to a potentially variable set of endogenously active
374 modulatory inputs, we transected the *ion*s and *son*s to obtain the same baseline
375 condition across preparations. However, this often results in a very slow pyloric rhythm,
376 or the pyloric rhythm shutting off entirely (Hamood et al., 2015; Zhang et al., 2009).
377 Therefore, to compare the variability of the pyloric rhythm during Gly^1-SIFamide to a
378 similarly robust pyloric rhythm, we included a comparison of the pyloric rhythm in saline
379 in the intact STNS, in addition to during saline superfusion after *ion*/*son* transection. In
380 an example experiment, the pyloric cycle period was approximately 1.6 s, with a CV of
381 0.02 (Fig. 1Ci, PD activity in the *pdn,* instantaneous cycle period plotted above traces).
382 After *ion*/*son* transection, the pyloric cycle period increased to ~ 2.4 s and a CV of 0.05

383 (Fig.1 Cii). During Gly^1-SIFamide, a gastric mill rhythm was activated, evident in LG and
384 DG neuron bursting (Fig. 1Ciii, *lgn, dgn* recordings) and longer duration gastric mill-
385 timed bursting in the IC neuron (*mvn*). Additionally, the LPG neuron switched from
386 pyloric-only activity (Fig. 1Ci-ii; *lpgn*, Saline conditions) to dual pyloric and gastric mill
387 (slow) bursting (Fig. 1Ciii). Although the average pyloric cycle period in Gly^1-SIFamide
388 (1.6 s) was similar to the intact STNS in this example, there was a visually evident
389 increase in variability (CV = 0.22) (Fig. 1Ciii). When quantified across preparations, we
390 found a consistent increase in pyloric cycle period variability in Gly^1-SIFamide compared
391 to Saline, including both Saline:Intact STNS and after Saline:*ion*/*son* cut (Fig. 1D) (One
392 Way RM ANOVA, $F(18,2) = 30.09$, $p < 0.001$, Table 1). In some experiments there was
393 no active pyloric rhythm to quantify in the Saline:*ions/sons* cut condition and thus points
394 between the Saline:Intact STNS and Gly^1-SIFamide conditions are connected without
395 an intermediate (Saline:*ion*s/*son*s cut) datapoint (see Methods). Thus, compared to the
396 pyloric rhythm when influenced by endogenously active modulatory inputs (Saline:Intact
397 STNS), or a slower pyloric rhythm in the absence of modulatory inputs, the pyloric
398 rhythm cycle period was more variable in the Gly^1-SIFamide modulatory state.

399

400 **Biphasic Regulation of the Pyloric Rhythm Frequency**

401 The larger pyloric cycle period CV during Gly^1-SIFamide application appeared to
402 be due to rhythmic changes in cycle period coinciding with activity in some of the gastric
403 mill neurons. Specifically, in an example experiment, the pyloric cycle period was longer
404 during times when the IC and LG neurons were active (Fig. 2A, pink box) relative to
405 pyloric activity when no gastric mill neuron was active (Fig. 2A; SIFbaseline; grey box;

406 dotted horizontal line across plot of instantaneous cycle period). Shorter duration pyloric
407 cycle periods relative to SIFbaseline coincided with LPG neuron slow bursts (Fig. 2A;
408 blue box).

409 To further examine the relationship between pyloric cycle period and gastric mill
410 neurons, we measured all pyloric cycle periods across the final 20 min steady-state of
411 30 min Gly^1-SIFamide (5 μM) bath applications and grouped them by the gastric mill
412 neurons that were active. Considering the four gastric mill neurons (LG, LPG, IC, DG),
413 plus the SIFbaseline condition in which no gastric mill neurons are active, there are 16
414 possible combinations of active gastric mill neurons during which a pyloric cycle period
415 might have occurred (Fig. 2B). We focused only on gastric mill-timed bursts (see
416 Methods; Fahoum and Blitz 2024), including for IC and LPG which express dual-
417 network activity. The average cycle period occurring during each neuron or combination
418 of neurons active, per experiment (black dots) and across all experiments (black bars)
419 are plotted for the 16 different combinations (Fig. 2B). Across 19 preparations, pyloric
420 cycle periods occurred during each of the 16 conditions in at least some preparations
421 (IC, LPG:IC, and LPG:DG:IC, n = 9-10; remaining 13 categories, n = 16-19). The total
422 number of pyloric cycles that occurred during each condition, across 19 preparations,
423 are indicated above the x axis labels (Fig. 2B; # cycles).

424 We first visually assessed cycle periods as a function of gastric mill neurons
425 active, using a dashed line to highlight the average cycle period across preparations
426 during the SIFbaseline, when no gastric mill neurons were active (grey region, dashed
427 line). Relative to this baseline, the average cycle period per experiment (dots) tended to
428 be shorter in duration than SIFbaseline during LPG activity, whether it was LPG alone

429 or in combination with DG and/or LG neurons (blue region), including the cumulative
430 average cycle period across preparations (black bars) (n = 16-19; Fig. 2B). Conversely,
431 average cycle periods during combinations of IC, DG, and LG activity (pink region)
432 tended to be longer, and thus above SIFbaseline in the graph, including the cumulative
433 average cycle period (IC, n = 9; IC:DG, IC:LG, IC:DG:LG, n = 19). This aligns with an
434 earlier study in which longer pyloric cycle periods correlated with longer duration IC
435 bursts (Blitz et al., 2019). Based on the number of cycles, IC gastric mill-timed bursts
436 most often coincided with LG activity (Fig. 2B, # cycles). During combinations that
437 included LPG plus IC or LPG plus IC and LG (IC:LPG, IC:LG:LPG, IC:DG:LPG, All
438 neurons, n = 10-19; purple regions), the average pyloric cycle period across
439 preparations was similar to SIFbaseline. Overall, this representation of cycle period as a
440 function of gastric mill neurons activity suggests that LPG, IC, and LG activity may be
441 responsible for the increased variability in pyloric cycle period during the Gly^1-SIFamide
442 gastric mill rhythm compared to saline (Fig. 1D). Further, effects of LPG versus IC, or IC
443 and LG, appear to offset the impact of the other neuron(s). That is, for example, during
444 conditions where LPG was active, pyloric cycle periods were shorter than SIFbaseline,
445 unless IC (or IC and LG) was active (purple regions). To analyze this data set
446 statistically, we used a mixed model ANOVA in order to accommodate the large number
447 of conditions, i.e., combinations of gastric mill neurons active, plus missing values for
448 some combinations (n = 9-19).

449 For the statistical analysis of gastric mill neuron activity on the pyloric cycle
450 period, we considered each gastric mill neuron to be a factor with a full 4-factor within-
451 subjects mixed model ANOVA, including all higher-order interactions. This model

452 indicated statistically significant effects of gastric mill neuron combinations on pyloric
453 cycle period variability ($X^2_{df = 15} = 102.57$, $p < 0.0001$). The model complexity was then
454 iteratively paired down, eliminating non-significant higher-order interactions (Table 2).
455 The most parsimonious model that still explained the variability in pyloric cycle period
456 included single factors LPG, IC, LG and 2-factor terms IC:LPG and IC:LG (Table 2). In
457 this model, there were significant interactions between LG and IC ($X^2_{df = 239} = 3.07$, $p =$
458 0.002) and between LPG and IC ($X^2_{df = 238} = -2.38$, $p = 0.02$). Specifically, LG had an
459 effect on pyloric cycle period when IC was firing a gastric mill burst ($p = 0.0011$, Table 2)
460 but not without IC gastric mill activity ($p = 0.40$, Table 2). However, IC had an effect on
461 cycle period with ($p<0.0001$) or without LG activity ($p=0.48$, Table 2), although a weaker
462 effect in the absence of LG. This points to IC playing an important role in the longer
463 cycle pyloric cycle periods, with possible assistance from LG. For the LPG and IC
464 interaction, LPG had an effect on pyloric cycle period with ($p < 0.0001$) or without ($p =$
465 0.0004, Table 2) IC generating a gastric mill burst. Similarly, IC affected the pyloric
466 cycle period with ($p = 0.008$) or without ($p < 0.0001$, Table 2) LPG firing a gastric mill
467 burst. Thus, from the overlap in timing and the preceding statistical analysis, it appears
468 that IC (possibly LG) and LPG are responsible for the increased and decreased cycle
469 period, respectively, and the consequent higher cycle period variability during the Gly^1-
470 SIFamide gastric mill rhythm. We therefore tested the roles of IC, LG, and LPG in
471 regulating pyloric cycle period by manipulating their activity.
472
473
474

475 **IC, but not LG, is responsible for longer pyloric cycle periods**

476 We first addressed whether IC and or LG were necessary for longer pyloric cycle
477 periods during the Gly[1]-SIFamide gastric mill rhythm. The pyloric cycle period was
478 variable in control conditions as is evident in two example experiments (Fig. 3Ai, Bi,
479 *pdn*, instantaneous cycle period plot above traces). This included longer pyloric cycle
480 periods during gastric mill-timed coactivity in LG and IC (Fig. 3; pink boxes). Identified
481 IC gastric mill bursts (see Methods) (Fahoum and Blitz, 2024), are marked with
482 brackets. In one instance in the time range shown, when LG fired a gastric mill burst,
483 but IC produced only pyloric-timed activity that did not reach the level of a gastric mill-
484 timed burst (Fig. 3Ai; grey box), there was no extension of the pyloric cycle period. This
485 is consistent with the statistical analysis of data from figure 2B, that LG had an effect on
486 pyloric cycle period, only when IC was also active (in gastric mill time). To test whether
487 IC and/or LG was responsible for the longer pyloric cycle periods, we reanalyzed a data
488 set from Fahoum and Blitz (2021) in which hyperpolarizing current (-2 to -4 nA) was
489 injected into either IC or LG neurons. In the example experiments, the much longer
490 cycle periods were eliminated when either LG or IC was hyperpolarized (Fig. 3Aii, Bii).
491 When IC was hyperpolarized, LG bursting persisted, and was qualitatively similar to pre-
492 hyperpolarization (Fig. 3Ai-ii). However, when LG was hyperpolarized, IC did not
493 generate any gastric mill-timed bursts, instead its activity was entirely pyloric-timed (Fig.
494 3Bii). Longer pyloric cycle periods, and therefore larger cycle period variability, returned
495 post hyperpolarization, as did IC gastric mill-timed bursting upon removal of
496 hyperpolarizing current into LG (Fig. 3Aiii, Biii).

497 To quantify the results of hyperpolarizing IC and LG, we measured pyloric cycle
498 period CV before (Pre), during (Hype) and after (Post) hyperpolarization (Fig. 4A). The
499 pyloric cycle period CV decreased when IC was hyperpolarized (Fig. 4Ai; black dots and
500 connecting lines indicate results from individual experiments, grey bars indicate
501 averages across experiments) (One Way RM ANOVA, $F(5,2) = 7.43$, $p = 0.01$, Table 3)
502 and when LG was hyperpolarized (Fig. 4Aii; One Way RM ANOVA, $F(3,2) = 6.09$, $p =$
503 0.04, Table 3). We also determined that the pyloric cycle period CV was not altered
504 when DG was hyperpolarized (Fig. 4Aiii; One Way RM ANOVA, $F(3,2) = 1.18$, $p = 0.37$,
505 Table 3) but it was lower when all three gastric mill neurons (IC, LG and DG) were
506 hyperpolarized (Fig. 4Aiv; One Way RM ANOVA, $F(5,2) = 9.13$, $p = 0.01$, Table 3). In
507 the cumulative data, a lower variability when IC or LG or the three gastric mill neurons
508 were hyperpolarized further indicated that IC and/or LG, but not DG, were responsible
509 for regulating pyloric cycle period. When LG was hyperpolarized, IC gastric mill bursting
510 was eliminated in the example experiment in figure 3B. Therefore, we aimed to quantify
511 IC and LG activity across all experiments when either LG or IC was hyperpolarized.
512 However, in 3/4 experiments there were no IC gastric mill bursts when LG was
513 hyperpolarized. Therefore, instead of quantifying IC gastric mill burst parameters, we
514 reported the number of IC gastric mill bursts before (Pre), during (Hype) and after (Post)
515 LG hyperpolarization (Fig. 4B). There was a reversible decrease in IC gastric mill bursts
516 with LG hyperpolarization (Fig. 4B) (One Way RM ANOVA, $F(3,2) = 22.75$, $p = 0.002$,
517 Table 3). In contrast, when IC was hyperpolarized, LG activity, including burst duration
518 (Fig. 4Ci), firing frequency (Fig. 4Cii) and number of spikes per burst (Fig. 4Ciii) did not
519 change (One Way RM ANOVA; $F(5,2) = 0.04 – 1.52$; all conditions, $p > 0.05$, Table 3).

520 Thus, LG impacts IC activity, but IC does not alter LG activity. It therefore appears likely
521 that hyperpolarizing LG eliminated extended pyloric cycle periods via elimination of IC
522 gastric mill bursting. In combination with a significant contribution of LG to pyloric cycle
523 period variability, only when IC is active (above) these results indicate that IC, but not
524 LG, gastric mill-timed bursts, is responsible for the longer pyloric cycle periods.

525

526 **LPG contributes to pyloric cycle period variability in Gly^1-SIFamide**

527 LPG gastric mill-timed activity correlated with decreased pyloric cycle periods
528 (Figs. 1, 2, 5). LPG is electrically coupled to the other pyloric pacemaker neurons (Fig.
529 1B) (Marder and Bucher, 2007; Shruti et al., 2014) and thus hyperpolarizing current
530 injection into the two LPG neurons could alter the pyloric cycle period. Therefore, to test
531 whether LPG was responsible for decreased pyloric cycle periods relative to
532 SIFbaseline (e.g., Fig. 5Ai), the two LPG neurons were photoinactivated (see Methods;
533 LPG:Kill) to selectively remove them from the network, and pyloric cycle periods during
534 Gly^1-SIFamide bath application were compared between LPG:Intact and LPG:Kill.
535 Photoinactivation of two neurons does not alter the response to bath-applied Gly^1-
536 SIFamide, and responses to two consecutive bath applications of Gly^1-SIFamide are not
537 different (Fahoum and Blitz, 2024).

538 In the absence of the LPG neurons (LPG:Kill), the pyloric cycle period variability
539 decreased (Fig. 5Aii) compared to the LPG:Intact condition. Eliminating LPG prevented
540 the periodic decreases in pyloric cycle period. Across experiments, the pyloric cycle
541 period CV was lower after LPG:Kill, compared to LPG:Intact (Fig. 5B; LPG:Intact [blue

542 dots] CV = 0.30 ± 0.03 ; LPG:Kill [black dots] CV = 0.11 ± 0.03; n = 9; two-tailed paired
543 t-test; t(8) = 7.78; p < 0.001). However, the decreased variability did not appear to be
544 due to only elimination of shorter pyloric cycle periods. The longer duration pyloric cycle
545 periods were also mostly eliminated in the LPG:Kill condition as can be seen in the
546 example experiment (Fig. 5Aii). Assessing regulation of pyloric cycle period across
547 preparations was complicated by the absence of LPG which eliminated several
548 combinations of active gastric mill neurons. Thus, we chose instead to examine the
549 distribution of cycle periods in the LPG:Intact vs LPG:Kill conditions. There is variability
550 in SIFbaseline pyloric cycle period across preparations (e.g., Fig. 2B, grey box), and
551 photoinactivation of the two LPG neurons shifted the SIFbaseline to shorter pyloric cycle
552 periods (compare instantaneous pyloric cycle period plot in Fig. 5Ai-ii), likely due to
553 removal of “electrical drag” on the pyloric pacemaker neuron AB (Kepler et al., 1990).
554 Thus, to determine whether there was any change in pyloric cycle period regulation
555 between the two conditions, we normalized each pyloric cycle period to the average
556 SIFbaseline cycle period in that preparation and accumulated all normalized pyloric
557 cycle period durations during each condition into their respective histograms (Fig. 5C)
558 (LPG:Intact, blue and LPG:Kill, grey). We also normalized pyloric cycle period count per
559 bin to the highest count for each condition to better enable comparison of the
560 histograms. In the LPG:Intact condition, in addition to the peak around 1 (SIFbaseline,
561 arrowhead), there were shorter pyloric cycle periods (<1; “Faster” bracket) and a
562 distributed set of bins at longer cycle periods (>1; “Slower” bracket) (Fig. 5C, blue
563 histogram). However, in the LPG:Kill condition (Fig. 5C, grey histogram), there was a
564 single grouping of bars centered around 1 (SIFbaseline) without a population of slower

565 or faster cycle periods. Therefore, removing LPG from the network prevented the
566 increase and the decrease in pyloric cycle period. Electrical coupling between LPG and
567 the pyloric pacemaker can explain why the pyloric rhythm was faster during the strong
568 depolarizations of LPG slow bursts. However, this does not explain why removing LPG
569 also eliminated slowing of the pyloric rhythm. Further, we showed above that IC gastric
570 mill bursting was responsible for extending the pyloric cycle period, slowing the rhythm
571 (Figs. 3-4). This combination of findings led us to ask whether photoinactivation of LPG
572 alters IC gastric mill activity.

573

574 **IC gastric mill bursts were not impacted by LPG photoinactivation**

575 As discussed previously, IC displays both pyloric- and gastric mill-timed bursts,
576 with a gastric mill burst often consisting of multiple pyloric-timed bursts (Fig. 6A). In an
577 example expanded region, a single IC gastric mill burst (Fig. 6Ai, brackets above *mvn*
578 recording) in the LPG:Intact condition consists of four pyloric-timed bursts (Fig. 6Ai,
579 brackets below *mvn* recording). In the LPG:Kill condition, based on established criteria
580 for IC gastric mill bursts (Blitz et al., 2019; Fahoum and Blitz, 2024), a single IC gastric
581 mill burst is approximately the same duration as in the LPG:Intact condition, but consists
582 of seven pyloric bursts, compared to four with LPG neurons intact (Fig. 6A). In a
583 previous study, there was no difference in IC activity between LPG:Intact and LPG:Kill,
584 including no difference in burst duration, firing frequency, and number of spikes per
585 burst for gastric mill bursts and for IC pyloric bursts within IC gastric mill bursts (Fahoum
586 and Blitz, 2024). Because our LPG:Intact, LPG:kill dataset was a subset from the
587 previous study (n = 9/11, see Methods), we reanalyzed the data to verify the result in

588 the specific experiments used here. We found no difference in number of IC gastric mill
589 bursts (Fig. 6Bi; Table 4), IC gastric mill burst duration (s) (Fig. 6Bii; Table 4), number of
590 IC spikes per gastric mill burst (Fig. 6Biii; Table 4), or firing frequency (Hz) (Fig. 6Biv;
591 Table 4). There was also no difference in the number of IC pyloric bursts (Fig. 6Ci;
592 Table 4), IC pyloric burst duration (s) (Fig. 6Cii; Table 4), or IC pyloric firing frequency
593 (Hz) (Fig. 6Civ; Table 4), although there was a trend toward shorter pyloric-timed burst
594 duration (Fig. 6Cii; Table 4), and there was a decrease in the number of spikes per
595 pyloric-timed burst (Fig. 6Ciii; Table 4). The difference between these results and the
596 previous study likely reflects the removal of two preparations in which there was little
597 pyloric regulation in the control condition. For the nine preparations in which there was
598 typical pyloric regulation in control, the tendency for IC pyloric bursts to be shorter, with
599 fewer action potentials in the LPG:Kill condition fits with the loss of long-duration pyloric
600 cycle periods. When longer pyloric cycle periods are eliminated, IC neuron pyloric
601 bursts are shortened as they are interrupted by inhibition from the pyloric pacemaker
602 ensemble at the start of each pyloric cycle (e.g., Fig. 6A). Importantly however, IC
603 gastric mill bursts were not altered by LPG:Kill and IC firing frequency, a measure of the
604 strength of neuronal activity, was not altered for IC gastric mill or pyloric bursts (Fig.
605 6Biv, Civ).

606

607 **Same IC activity level does not slow the pyloric rhythm in the LPG:Kill condition**

608 To determine the relationship between the strength (firing frequency) of IC gastric
609 mill bursts and pyloric cycle period before versus after LPG:Kill, we plotted
610 instantaneous pyloric cycle period against IC firing frequency (Hz) for all pyloric cycles

611 across a 20 min steady state region of Gly^1-SIFamide application for each of nine
612 preparations (Fig. 7). Within a preparation, across the same IC firing frequencies, there
613 were many longer duration pyloric cycle periods in LPG:Intact (blue circles) but many
614 fewer longer duration cycles in the LPG:Kill condition (grey circles) (Fig. 7; n = 9). This
615 indicated that LPG was playing a major role in the ability of IC to increase pyloric cycle
616 period. The occasional ability of IC to increase pyloric cycle period in the absence of
617 LPG indicated a weaker, or only occasionally modulated, connection to the other pyloric
618 pacemaker neurons (PD and AB) (Figs. 7, 8). These data thus suggest that while IC
619 activity strength is not affected by LPG photoinactivation, its ability to slow the pyloric
620 rhythm requires the presence of LPG.

621

622

623 **Discussion**

624 In this study, we show that the frequency of the faster pyloric rhythm varies
625 between three levels in time with different components of the related, slower gastric mill
626 rhythm during the Gly^1-SIFamide neuropeptide modulatory state. The LPG neuron
627 switches from pyloric-only activity to dual pyloric and gastric mill activity during Gly^1-
628 SIFamide application (Fahoum and Blitz, 2024, 2021; Snyder and Blitz, 2022).
629 Surprisingly, we found that this dual-network LPG neuron is necessary for both
630 decreasing and increasing the pyloric frequency. This occurs due to LPG intrinsic
631 gastric mill-timed bursts directly increasing the frequency of the pyloric pacemaker
632 neuron oscillations, and the IC neuron indirectly slowing the pyloric pacemaker
633 oscillations primarily via its chemical synaptic inhibition of LPG. This complex biphasic

634 regulation of a related network is distinct in both form and mechanism from previous
635 examples of internetwork coordination in the STNS during other modulatory states,
636 emphasizing the flexible nature of such coordination.

637

638 **Coordination of Related Behaviors**

639 There are multiple ways in which coordination occurs between different
640 behaviors and between their underlying CPG networks. Here we focused on a single
641 modulatory state and how the activity of one network varies within a single cycle of a
642 second network's activity. Unlike other gastric mill rhythm versions, the Gly^1-SIFamide
643 gastric mill rhythm is triphasic (Blitz et al., 2019; Fahoum and Blitz, 2024). During this
644 triphasic gastric mill rhythm, there is a "baseline" pyloric frequency due to Gly^1-
645 SIFamide modulatory actions, and the pyloric rhythm is regulated away from this
646 baseline in opposing directions during different phases of the slower gastric mill rhythm.
647 The specific behavioral reason for phasic increases and decreases in pyloric frequency
648 during the Gly^1-SIFamide rhythm is not known. In general, food is mechanically broken
649 down by teeth within the gastric mill region, moves through the cardiopyloric valve into
650 the pyloric chamber, and is filtered in the pylorus before moving into the midgut for
651 chemical digestion and absorption of nutrients (Heinzel et al., 1993; Selverston and
652 Moulins, 1987). Larger particles can be moved back into the gastric mill chamber for
653 further processing by the teeth (McGaw and Curtis, 2013). Different rates of pyloric
654 contractions during different gastric mill phases might facilitate movements through the
655 valve with optimal timing relative to teeth movements, either chewed food into the
656 pylorus, or larger particles and gastric juices back into the gastric mill chamber.

657 However, these are only speculations, as the complexity of teeth movements along
658 multiple axes, plus the convoluted folds, many bristles/filtering apparatus and overall
659 three-dimensional shape of the pyloric chamber make it difficult to determine the
660 implications of coordination between these regions (Heinzel, 1988; Heinzel et al., 1993;
661 Selverston and Moulins, 1987). Although difficult to assess the behavioral roles,
662 coordination does appear to be important for these related behaviors as it occurs during
663 multiple modulatory states in vitro and in vivo (Bartos et al., 1999; Bartos and Nusbaum,
664 1997; Clemens et al., 1998a, 1998b; Stein and Harzsch, 2021; Wood et al., 2004).

665 Other gastric mill rhythm versions are biphasic, and when pyloric rhythm
666 variability has been quantified, the pyloric frequency during one phase of the gastric mill
667 rhythm is at a “baseline” frequency due to modulatory input, and regulated away from
668 this baseline during the other phase of the gastric mill rhythm (Bartos and Nusbaum,
669 1997). A cellular mechanism identified for this coordination is that a gastric mill neuron
670 provides local, presynaptic inhibition of a modulatory neuron, decreasing modulatory
671 excitation of the pyloric network during one phase of the gastric mill rhythm (Bartos and
672 Nusbaum, 1997; Coleman et al., 1995; Coleman and Nusbaum, 1994; Nusbaum et al.,
673 1992). Thus, there is indirect communication between the two networks via a local
674 feedback synapse. Indirect interactions between networks can also occur via long-
675 distance feedback from network neurons to modulatory inputs or via motor efference
676 copy to related networks (Blitz and Nusbaum, 2008; Lambert et al., 2023; Wood et al.,
677 2004). Although there are both local and long-distance feedback projections to the
678 source of Gly^1-SIFamide (MCN5) (Blitz et al., 2019; Norris et al., 1996), they do not
679 contribute to the internetwork regulation described here, as the neuropeptide was bath-

680 applied. Instead, we found that synapses between network neurons underly biphasic
681 regulation of the pyloric rhythm.

682 In addition to phasic coordination, there may be correlated changes in the overall
683 activity levels of related networks such as increased respiratory activity to match more
684 intense forms of locomotion, or increased swallowing frequency to match increased
685 chewing rates (Hao et al., 2021; Hérent et al., 2023). In the crustacean STNS, when the
686 pyloric and gastric mill networks are both active, their activity level is coordinated such
687 that faster pyloric rhythms occur with faster gastric mill rhythms (Bartos et al., 1999;
688 Powell et al., 2021; Saideman et al., 2007). Correlated changes in frequency and/or
689 strength can reflect common inputs. In the crab STNS, the modulatory neuron MCN1
690 acts on both networks, and increasing MCN1 firing frequency speeds both rhythms
691 (Bartos et al., 1999; Bartos and Nusbaum, 1997). Similarly, in lamprey, rodents, and
692 cats, the mesencephalic locomotor region provides parallel input to respiratory and
693 locomotor CPGs (Hérent et al., 2023; Juvin et al., 2022; Ryczko and Dubuc, 2013).

694 Some related behaviors display coupling of their activity, with a discrete number
695 of cycles of one pattern occurring relative to a full cycle of the other pattern. Coupling
696 occurs between locomotion and chewing, and locomotion and respiration in humans,
697 other mammals and birds; between whisking and respiration in rodents; and between
698 pyloric and gastric mill rhythms in crustaceans (Bartos et al., 1999; Clemens et al.,
699 1998a; Juvin et al., 2022; Maezawa et al., 2020; Moore et al., 2013; Powell et al., 2021).
700 Coupling of rhythmic behaviors may arise from mechanical forces. For example, flight
701 muscle attachment to structures essential for respiration in birds, and the movement of
702 internal organs in galloping horses may contribute to coupling between locomotion and

703 respiration (Juvin et al., 2022). Similarly, accessory teeth movements are mechanically
704 coupled to the cardiopyloric valve in the stomatogastric system (McGaw and Curtis,
705 2013). However, direct synaptic connections between CPGs can also contribute to this
706 type of internetwork coordination (Juvin et al., 2022). In rodents, proper timing of
707 swallowing within the respiratory cycle, and 1:1 coupling of whisking and fast sniffing,
708 appear to be due to synapses between these related CPGs (Huff et al., 2022; Moore et
709 al., 2013). These coupling ratios between networks are not fixed and can vary during
710 different forms of locomotion, or different breathing behaviors such as fast sniffing and
711 slow breathing (Juvin et al., 2022; Moore et al., 2013; Saunders et al., 2004). In the crab
712 STNS, a direct inhibitory synapse from the pyloric pacemaker neuron onto one of the
713 gastric mill CPG neurons is essential for coupling between the pyloric and gastric mill
714 rhythms driven by the modulatory neuron MCN1. This internetwork synapse allows the
715 pyloric rhythm to control the speed of the gastric mill rhythm (Bartos et al., 1999; Nadim
716 et al., 1998). However, during the Gly^1-SIFamide rhythm, the speed of the pyloric
717 rhythm does not regulate LPG gastric mill bursting, reinforcing the flexible nature of
718 internetwork coordination (Fahoum and Blitz, 2024).

719

720 **Electrical and Chemical Transmission Mediate Coordination**

721 Due to the well-described small networks in the STNS, we were able to ascertain
722 the cellular mechanisms underlying the biphasic internetwork interactions. During Gly^1-
723 SIFamide application, IC gastric mill bursting is necessary for prolonging the pyloric
724 cycle period. Hyperpolarizing the IC neuron eliminated longer pyloric cycle periods,
725 even if LG, the other neuron typically active during longer pyloric cycle periods, was still

726 bursting. Periodic long-duration IC bursts also inhibit the pyloric rhythm during activation
727 of another STNS modulatory neuron, MCN7, which releases the neuropeptide proctolin,
728 although the particular IC target(s) among the five-neuron pyloric pacemaker ensemble
729 (1 copy of AB, 2 copies each of PD and LPG) was not determined (Blitz et al., 1999). It
730 was recently determined that Gly^1-SIFamide enhances a typically ineffective IC to LPG
731 synapse (Fahoum and Blitz, 2023). IC chemical synapses within the STG, including the
732 IC to LPG synapse, are fast inhibitory glutamatergic connections that are blocked by the
733 chloride channel blocker picrotoxin (Fahoum and Blitz, 2024; Marder and Bucher,
734 2007). Inhibitory neuron connections between networks are implicated in other
735 internetwork interactions, although further exploration is still needed for a mechanistic
736 understanding at the cellular level (Huff et al., 2022). Unexpectedly, photoinactivation of
737 LPG almost entirely eliminates IC inhibition of the pyloric pacemaker neurons, despite
738 no change in the strength of IC activity. This result indicates that the modulated IC to
739 LPG synapse is primarily responsible for IC inhibition of the pyloric rhythm, although
740 there may be an additional small contribution of an IC to AB and/or PD synapse, at least
741 in some preparations (Fig. 8). In most modulatory conditions, the AB neuron is the
742 conditional oscillator, and PD and LPG are co-active due to electrical coupling among
743 this five-neuron ensemble (Marder and Bucher, 2007). LPG to PD and LPG to AB
744 synapses are rectifying such that hyperpolarizing current flows preferentially from LPG
745 to PD and AB (Shruti et al., 2014) (Fahoum, Nadim, Blitz unpublished). Due to this
746 directional electrical coupling, IC inhibition of LPG, during longer-duration gastric mill IC
747 bursts, inhibits LPG to directly regulate LPG gastric mill-timed activity (Fahoum and
748 Blitz, 2024), and indirectly inhibit the pyloric pacemakers to slow the pyloric rhythm

749 during the IC:LG phase of the Gly[1]-SIFamide gastric mill rhythm. The reason for the
750 “funneling” of IC chemical inhibition through the electrical synapse from LPG to AB/PD
751 is not known. However, it may represent a conservation of function with the IC to LPG
752 synapse playing roles in both gastric mill pattern generation as well as its coordination
753 with the pyloric network.

754 Dual-network activity under particular modulatory conditions is common among
755 related networks (Bartlett and Leiter, 2012; Dickinson, 1995; Hooper and Moulins, 1990;
756 Koch et al., 2011; Meyrand et al., 1994; Tryba et al., 2008). While this typically occurs
757 due to internetwork synapses, the LPG neuron dual-activity occurs via modulation of
758 LPG intrinsic properties. LPG retains its pyloric-timed activity because of its electrical
759 coupling to the other pacemaker neurons and then periodically generates slower, longer
760 duration gastric mill-timed bursts via intrinsic voltage-dependent currents (Fahoum and
761 Blitz, 2021; Snyder and Blitz, 2022). During LPG gastric mill bursts, the LPG membrane
762 potential remains depolarized across multiple pyloric cycles. Our results here indicate
763 that a sufficient amount of current during this maintained depolarization passes into
764 AB/PD to increase pyloric rhythm frequency, despite the rectification in which
765 depolarizing current flows better from AB/PD to LPG. Electrical synapses are subject to
766 modulation (Kothmann et al., 2009; Lane et al., 2018; O’Brien, 2014). It is possible that
767 Gly[1]-SIFamide modulates the LPG to AB/PD electrical synapses to decrease or
768 eliminate the rectification. However, there does not appear to be any change in
769 electrical coupling strength or rectification during Gly[1]-SIFamide application (Fahoum,
770 Nadim, Blitz, unpublished). Electrical synapses alone and in combination with chemical
771 synapses can have surprising and complex effects on network outputs (Alcamí and

772 Pereda, 2019; Connors, 2017; Marder et al., 2017; Vaughn and Haas, 2022).
773 Rectification of electrical synapses occurs to different extents and can further add to the
774 complexity of electrical synapse contributions, such as enabling coincidence detection
775 and amplification of chemical synapses, and shaping network sensitivity to chemical
776 synapses (Connors, 2017; Edwards et al., 1998; Gutierrez and Marder, 2013; Liu et al.,
777 2017; Mendoza and Haas, 2022; Palacios-Prado et al., 2014; Rash et al., 2013; Vaughn
778 and Haas, 2022).

779 Here we find that the same rectifying electrical synapse alternately reinforces and
780 diminishes modulatory neuropeptide effects on network frequency. These actions occur
781 due to intrinsic currents enabling reinforcement, and chemical synaptic currents leading
782 to diminished peptide actions. LPG thus serves as a point of convergence for
783 coordination, despite the two network interactions acting in opposite directions. Due to
784 the fluid nature of network composition, dual-network neurons such as LPG provide
785 flexibility by adding and subtracting their activity to different behavioral outputs
786 (Ainsworth et al., 2011; Clapp et al., 2011; Dickinson et al., 1990; Hooper and Moulins,
787 1989; Roopun et al., 2008; Weimann et al., 1991). Additionally, dual-network neurons
788 can provide flexibility in coordinating network activity by serving as a variable link
789 between networks. This ability however depends on whether they are recruited into new
790 networks as passive followers, or as active components with sufficient synaptic access
791 to a new network to mediate coordination (Fahoum and Blitz, 2024, 2023; Hooper and
792 Moulins, 1990).

793 Dysfunctional internetwork coordination can impact health and well-being, such
794 as an insufficient oxygen supply relative to metabolic demand if respiration is not

795 coordinated with other motor activity, decreased food intake or choking due to improper
796 coordination of breathing and swallowing, or disrupted communication abilities arising
797 from problems coordinating vocalization and respiration (Barlow, 2009; Juvin et al.,
798 2022; Yagi et al., 2017). Thus, it is important to continue adding to our understanding of
799 internetwork coordination among the many behaviors that require coordination,
800 including understanding how coordination varies across behavioral and environmental
801 conditions (Clemens et al., 1998b; Juvin et al., 2022; Stein and Harzsch, 2021; Stickford
802 and Stickford, 2014).

803

804

805 Ainsworth M, Lee S, Cunningham MO, Roopun AK, Traub RD, Kopell NJ, Whittington
806 MA (2011) Dual gamma rhythm generators control interlaminar synchrony in
807 auditory cortex. J Neurosci 31:17040–17051.

808 Alcamí P, Pereda AE (2019) Beyond plasticity: the dynamic impact of electrical
809 synapses on neural circuits. Nat Rev Neurosci 20:253–271.

810 Anderson T, Garcia AJ, Baertsch NA, Pollak J, Bloom JC, Wei AD, Rai KG, Ramirez JM
811 (2016) A novel excitatory network for the control of breathing. Nature 536:76–80.

812 Barlow SM (2009) Central pattern generation involved in oral and respiratory control for
813 feeding in the term infant. Curr Opin Otolaryngol Head Neck Surg 17:187–193.

814 Barnett WH, Baekey DM, Paton JFR, Dick TE, Wehrwein EA, Molkov YI (2021)
815 Heartbeats entrain breathing via baroreceptor-mediated modulation of expiratory
816 activity. Exp Physiol 106:1181–1195.

817 Bartlett D, Leiter JC (2012) Coordination of breathing with nonrespiratory activities.
818 Comp Physiol 2:1387–1415.

819 Bartos M, Manor Y, Nadim F, Marder E, Nusbaum MP (1999) Coordination of fast and
820 slow rhythmic neuronal circuits. J Neurosci 19:6650–6660.

821 Bartos M, Nusbaum MP (1997) Intercircuit control of motor pattern modulation by
822 presynaptic inhibition. J Neurosci 17:2247–2256.

823 Beenhakker MP, Blitz DM, Nusbaum MP (2004) Long-Lasting Activation of Rhythmic
824 Neuronal Activity by a Novel Mechanosensory System in the Crustacean
825 Stomatogastric Nervous System. J Neurosci 91:78–91.

826 Blitz DM (2023) Neural circuit regulation by identified modulatory projection neurons.
827 Front Neurosci 17.

828 Blitz DM, Christie AE, Coleman MJ, Norris BJ, Marder E, Nusbaum MP (1999) Different
829 proctolin neurons elicit distinct motor patterns from a multifunctional neuronal
830 network. J Neurosci 19:5449–5463.

831 Blitz DM, Christie AE, Cook AP, Dickinson PS, Nusbaum MP (2019) Similarities and
832 differences in circuit responses to applied Gly^1-SIFamide and peptidergic (Gly^1 -
833 SIFamide) neuron stimulation. J Neurophysiol 121:950–972.

834 Blitz DM, Nusbaum MP (2008) State-dependent presynaptic inhibition regulates central
835 pattern generator feedback to descending inputs. J Neurosci 28:9564–9574.

836 Blitz DM, White RS, Saideman SR, Cook A, Christie AE, Nadim F, Nusbaum MP (2008)
837 A newly identified extrinsic input triggers a distinct gastric mill rhythm via activation
838 of modulatory projection neurons. J Exp Biol 211:1000–1011.

839 Bucher D, Haspel G, Golowasch J, Nadim F (2015) Central pattern generators In: ELS ,
840 John Wiley & Sons, Ltd: Chichester.

841 Cao Y, Roy S, Sachdev RNS, Heck DH (2012) Dynamic Correlation between Whisking
842 and Breathing Rhythms in Mice. J Neurosci 32:1653–1659.

843 Christie AE, Stein W, Quinlan JE, Beenhakker MP, Marder E, Nusbaum MP (2004)
844 Actions of a histaminergic/peptidergic projection neuron on rhythmic motor patterns
845 in the stomatogastric nervous system of the crab *Cancer borealis*. J Comp Neurol
846 469:153–169.

847 Clapp WC, Rubens MT, Sabharwal J, Gazzaley A (2011) Deficit in switching between
848 functional brain networks underlies the impact of multitasking on working memory
849 in older adults. Proc Natl Acad Sci U S A 108:7212–7217.

850 Clemens S, Combes D, Meyrand P, Simmers J (1998a) Long-term expression of two
851 interacting motor pattern-generating networks in the stomatogastric system of freely
852 behaving lobster. J Neurophysiol 79:1396–1408.

853 Clemens S, Massabuau JC, Legeay A, Meyrand P, Simmers J (1998b) In vivo
854 modulation of interacting central pattern generators in lobster stomatogastric
855 ganglion: influence of feeding and partial pressure of oxygen. J Neurosci 18:2788–
856 2799.

857 Coleman MJ, Meyrand P, Nusbaum MP (1995) A switch between two modes of
858 synaptic transmission mediated by presynaptic inhibition. Nature 378:502–505.

859 Coleman MJ, Nusbaum MP (1994) Functional consequences of compartmentalization
860 of synaptic input. J Neurosci 14:6544–6552.

861 Connors BW (2017) Synchrony and so much more: Diverse roles for electrical synapses
862 in neural circuits. Dev Neurobiol 77:610–624.

863 Daley MA, Bramble DM, Carrier DR (2013) Impact Loading and Locomotor-Respiratory
864 Coordination Significantly Influence Breathing Dynamics in Running Humans. PLoS
865 One 8:70752.

866 Daur N, Nadim F, Bucher D (2016) The complexity of small circuits: the stomatogastric
867 nervous system. Curr Opin Neurobiol 41:1–7.

868 Demartsev V, Manser MB, Tattersall GJ (2022) Vocalization-associated respiration
869 patterns: thermography-based monitoring and detection of preparation for calling. J
870 Exp Biol 225.

871 Dickinson PS (1995) Interactions among neural networks for behavior. Curr Op
872 Neurobiol 5:792–798.

873 Dickinson PS, Mecsas C, Marder E (1990) Neuropeptide fusion of two motor-pattern
874 generator circuits. Nature 344:155–157.

875 Dickinson PS, Stemmler EA, Cashman CR, Brennan HR, Dennison B, Huber KE,
876 Peguero B, Rabacal W, Goiney CC, Smith CM, Towle DW, Christie AE (2008)

877 SIFamide peptides in clawed lobsters and freshwater crayfish (Crustacea,
878 Decapoda, Astacidea): A combined molecular, mass spectrometric and
879 electrophysiological investigation. Gen and Comp Endocrinol 156:347–360.

880 Edwards DH, Yeh SR, Krasne FB (1998) Neuronal coincidence detection by voltage-
881 sensitive electrical synapses. Proc Natl Acad Sci U S A 95:7145–7150.

882 Fahoum S-RH, Blitz DM (2024) Switching neuron contributions to second network
883 activity. J Neurophysiol 131:417–434.

884 Fahoum S-RH, Blitz DM (2023) Parallel Peptide Actions Underlie Recruitment and
885 Coordination of a Dual-Network Neuron. bioRxiv 2023.12.15.571956.

886 Fahoum S-RH, Blitz DM (2021) Neuronal switching between single- and dual-network
887 activity via modulation of intrinsic membrane properties. J Neurosci 41:7848–7863.

888 Fortune ES, Rodríguez C, Li D, Ball GF, Coleman MJ (2011) Neural mechanisms for
889 the coordination of duet singing in wrens. Science (1979) 334:666–670.

890 Gariépy JF, Missaghi K, Dubuc R (2010) The interactions between locomotion and
891 respiration. Prog Brain Res 187:173–188.

892 Grillner S, El Manira A (2020) Current principles of motor control, with special reference
893 to vertebrate locomotion. Physiol Rev 100:271–320.

894 Gutierrez GJ, Grashow RG (2009) *Cancer borealis* stomatogastric nervous system
895 dissection. J Vis Exp 23:1–5.

896 Gutierrez GJ, Marder E (2013) Rectifying electrical synapses can affect the influence of
897 synaptic modulation on output pattern robustness. J Neurosci 33:13238–13248.

898 Hamood AW, Haddad SA, Otopalik AG, Rosenbaum P, Marder E (2015) Quantitative
899 reevaluation of the effects of short- and long-term removal of descending
900 modulatory inputs on the pyloric rhythm of the crab, *Cancer borealis*. eNeuro 2:1–
901 13.

902 Hao N, Sasa A, Kulvanich S, Nakajima Y, Nagoya K, Magara J, Tsujimura T, Inoue M
903 (2021) Coordination of Respiration, Swallowing, and Chewing in Healthy Young
904 Adults. Front Physiol 12:696071.

905 Heinzel HG (1988) Gastric mill activity in the lobster. I. Spontaneous modes of chewing.
906 J Neurophysiol 59:528–550.

907 Heinzel HG, Weimann JM, Marder E (1993) The behavioral repertoire of the gastric mill
908 in the crab, *Cancer pagurus*: an in situ endoscopic and electrophysiological
909 examination. J Neurosci 13:1793.

910 Hérent C, Diem S, Usseglio G, Fortin G, Bouvier J (2023) Upregulation of breathing rate
911 during running exercise by central locomotor circuits in mice. Nat Commun 14:2–
912 17.

913 Higashino M, Miyata K, Kudo K (2022) Coordination dynamics of thoracic and
914 abdominal movements during voluntary breathing. Sci Rep 12:13266.

915 Hooper SL, Moulins M (1990) Cellular and synaptic mechanisms responsible for a long-
916 lasting restructuring of the lobster pyloric network. J Neurophysiol 64:1574.

917 Hooper SL, Moulins M (1989) Switching of a neuron from one network to another by
918 sensory-induced changes in membrane properties. Science (1979) 244:1587–
919 1589.

920 Hooper SL, Thuma JB, Guschlbauer C, Schmidt J, Büschges A (2015) Cell dialysis by
921 sharp electrodes can cause nonphysiological changes in neuron properties. J
922 Neurophysiol 114:1255–1271.

923 Huff A, Karlen-Amarante M, Pitts T, Marino Ramirez J (2022) Optogenetic stimulation of
924 pre-Botzinger complex reveals novel circuit interactions in swallowing-breathing
925 coordination. PNAS 119:1–11.

926 Huybrechts J, Nusbaum MP, Bosch L Vanden, Baggerman G, De Loof A, Schoofs L
927 (2003) Neuropeptidomic analysis of the brain and thoracic ganglion from the Jonah
928 crab, *Cancer borealis*. Biochem Biophys Res Commun 308:535–544.

929 Juvin L, Colnot E, Barrière G, Thoby-Brisson M, Morin D (2022) Neurogenic
930 mechanisms for locomotor-respiratory coordination in mammals. Front Neuroanat
931 16.

932 Kepler TB, Marder EVE, Abbott LF (1990) The effect of electrical coupling on the
933 frequency of model neuronal oscillators. Science (1979) 248:83–85.

934 Koch H, Garcia AJ, Ramirez J-M (2011) Network reconfiguration and neuronal plasticity
935 in rhythm-generating networks. Integr Comp Biol 51:856–868.

936 Kothmann WW, Massey SC, O'Brien J (2009) Dopamine-stimulated dephosphorylation
937 of connexin 36 mediates AII amacrine cell uncoupling. J Neurosci 29:14903–14911.

938 Lambert FM, Beraneck M, Straka H, Simmers J (2023) Locomotor efference copy
939 signaling and gaze control: An evolutionary perspective. Curr Opin Neurobiol 82.

940 Lane BJ, Kick DR, Wilson DK, Nair SS, Schulz DJ (2018) Dopamine maintains network
941 synchrony via direct modulation of gap junctions in the crustacean cardiac
942 ganglion. Elife 7:e39368.

943 Liu P, Chen B, Mailler R, Wang ZW (2017) Antidromic-rectifying gap junctions amplify
944 chemical transmission at functionally mixed electrical-chemical synapses. Nat
945 Commun 8:14818.

946 Maezawa H, Koganemaru S, Matsuhashi M, Hirata M, Funahashi M, Mima T (2020)
947 Entrainment of chewing rhythm by gait speed during treadmill walking in humans.
948 Neurosci Res 156:88–94.

949 Marder E, Bucher D (2007) Understanding circuit dynamics using the stomatogastric
950 nervous system of lobsters and crabs. Ann Rev Physiol 69:291–316.

951 Marder E, Gutierrez GJ, Nusbaum MP (2017) Complicating connectomes: Electrical
952 coupling creates parallel pathways and degenerate circuit mechanisms. Dev
953 Neurobiol 77:597–609.

954 McGaw IJ, Curtis DL (2013) A review of gastric processing in decapod crustaceans. J
955 Comp Physiol B 183:443–465.

956 Mendoza AJ, Haas JS (2022) Intrinsic Sources and Functional Impacts of Asymmetry at
957 Electrical Synapses. eNeuro 9:1–14.

958 Meyrand P, Simmers J, Moulins M (1994) Dynamic construction of a neural network
959 from multiple pattern generators in the lobster stomatogastric nervous system. J
960 Neurosci 14:630–644.

961 Moore JD, Deschênes M, Furuta T, Huber D, Smear MC, Demers M, Kleinfeld D (2013)
962 Hierarchy of orofacial rhythms revealed through whisking and breathing. Nature
963 2013 497:7448 497:205–210.

964 Mulloney B, Smarandache-Wellmann C (2012) Neurobiology of the crustacean
965 swimmeret system. Prog Neurobiol 96:242–267.

966 Nadim F, Manor Y, Nusbaum MP, Marder E (1998) Frequency regulation of a slow
967 rhythm by a fast periodic input. J Neurosci 18:5053–5067.

968 Norris BJ, Coleman MJ, Nusbaum MP (1996) Pyloric motor pattern modification by a
969 newly identified projection neuron in the crab stomatogastric nervous system. J
970 Neurophysiol 75:97–108.

971 Nusbaum MP, Beenhakker MP (2002) A small-systems approach to motor pattern
972 generation. Nature 417:343–350.

973 Nusbaum MP, Weimann JM, Golowasch J, Marder E (1992) Presynaptic control of
974 modulatory fibers by their neural network targets. J Neurosci 12:2706–2714.

975 O'Brien J (2014) The ever-changing electrical synapse. Curr Opin Neurobiol 29:64–72.

976 Okobi DE, Banerjee A, Matheson AMM, Phelps SM, Long MA (2019) Motor cortical
977 control of vocal interaction in neotropical singing mice. Science (1979) 363:983–
978 988.

979 Palacios-Prado N, Huetteroth W, Pereda AE (2014) Hemichannel composition and
980 electrical synaptic transmission: molecular diversity and its implications for
981 electrical rectification. Front Cell Neurosci 8:324.

982 Powell D, Haddad SA, Gorur-Shandilya S, Marder E (2021) Coupling between fast and
983 slow oscillator circuits in *Cancer borealis* is temperature-compensated. Elife
984 10:e60454.

985 Ramirez J-M, Baertsch N (2018) Defining the rhythmogenic elements of mammalian
986 breathing. Physiology 33:302–316.

987 Rash JE, Curti S, Vanderpool KG, Kamasawa N, Nannapaneni S, Palacios-Prado N,
988 Flores CE, Yasumura T, O'Brien J, Lynn BD, Bukauskas FF, Nagy JI, Pereda AE
989 (2013) Molecular and Functional Asymmetry at a Vertebrate Electrical Synapse.
990 Neuron 79:957–969.

991 Roopun AK, Kramer MA, Carracedo LM, Kaiser M, Davies CH, Traub RD, Kopell NJ,
992 Whittington MA (2008) Temporal interactions between cortical rhythms. Front
993 Neurosci 2:145–154.

994 Ryczko D, Dubuc R (2013) The multifunctional mesencephalic locomotor region. Curr
995 Pharm Des 19:4448–4470.

996 Saideman SR, Blitz DM, Nusbaum MP (2007) Convergent motor patterns from
997 divergent circuits. J Neurosci 27:6664–6674.

998 Saunders SW, Rath D, Hodges PW (2004) Postural and respiratory activation of the
999 trunk muscles changes with mode and speed of locomotion. Gait Posture 20:280–
1000 290.

1001 Selverston A, Moulins M (1987) The Crustacean Stomatogastric System, The
1002 Crustacean Stomatogastric System. Springer Berlin Heidelberg.

1003 Shruti S, Schulz DJ, Lett KM, Marder E (2014) Electrical coupling and innexin
1004 expression in the stomatogastric ganglion of the crab *Cancer borealis*. J
1005 Neurophysiol 112:2946–2958.

1006 Sillar KT, Simmers J, Combes D (2023) From tadpole to adult frog locomotion. Curr
1007 Opin Neurobiol 82:102753.

1008 Snyder RR, Blitz DM (2022) Multiple intrinsic membrane properties are modulated in a
1009 switch from single- to dual-network activity. J Neurophysiol 128:1181–1198.

1010 Spencer RM, Blitz DM (2016) Network feedback regulates motor output across a range
1011 of modulatory neuron activity. J Neurophysiol 115:3249–3263.

1012 Stein W, Harzsch S (2021) The neurobiology of ocean change – insights from decapod
1013 crustaceans. Zoology 144:125887.

1014 Stickford ASL, Stickford JL (2014) Ventilation and locomotion in humans: Mechanisms,
1015 implications, and perturbations to the coupling of these two rhythms. Springer Sci
1016 Rev 2:95–118.

1017 Tryba AK, Peña F, Lieske SP, Viemari J-C, Thoby-Brisson M, Ramirez J-M (2008)
1018 Differential modulation of neural network and pacemaker activity underlying eupnea
1019 and sigh-breathing activities. J Neurophysiol 99:2114–2125.

1020 Vaughn MJ, Haas JS (2022) On the diverse functions of electrical synapses. Front Cell
1021 Neurosci 16.

1022 Wei XP, Collie M, Dempsey B, Fortin G, Yackle K (2022) A novel reticular node in the
1023 brainstem synchronizes neonatal mouse crying with breathing. Neuron 110:644-
1024 657.e6.

1025 Weimann JM, Meyrand P, Marder E (1991) Neurons that form multiple pattern
1026 generators: Identification and multiple activity patterns of gastric/pyloric neurons in
1027 the crab stomatogastric system. J Neurophysiol 65:111–122.

1028 Wood DE, Manor Y, Nadim F, Nusbaum MP (2004) Intercircuit control via rhythmic
1029 regulation of projection neuron activity. J Neurosci 24:7455–7463.

1030 Yagi N, Oku Y, Nagami S, Yamagata Y, Kayashita J, Ishikawa A, Domen K, Takahashi
1031 R (2017) Inappropriate Timing of Swallow in the Respiratory Cycle Causes
1032 Breathing-Swallowing Discoordination. Front Physiol 8:676.

1033 Yasuda A, Yasuda-Kamatani Y, Nozaki M, Nakajima T (2004) Identification of
1034 GYRKPPFNGSIFamide (crustacean-SIFamide) in the crayfish *Procambarus clarkii*
1035 by topological mass spectrometry analysis. Gen and Comp Endocrinol 135:391–
1036 400.

1037 Zhang Y, Khorkova O, Rodriguez R, Golowaschi J (2009) Activity and neuromodulatory
1038 input contribute to the recovery of rhythmic output after decentralization in a central
1039 pattern generator. J Neurophysiol 101:372–386.

1040

1041

1042 **Figure Legends**

1043 **Figure 1. Gly^1-SIFamide elicited a variable pyloric rhythm**. ***A*,** Schematic of the
1044 isolated stomatogastric nervous system (STNS) of the crab, *Cancer borealis*. The STNS
1045 consists of the paired commissural ganglia (CoG), the single oesophageal ganglion
1046 (OG) and the single stomatogastric ganglion (STG), plus motor and connecting nerves.
1047 The STG consists of neuropil and the cell bodies of both the gastric mill and pyloric
1048 network neurons. The line breaks on the *ion* and *son* indicates where they were cut to
1049 isolate the STG network (Saline:*ions/sons* cut). Two compartments were created with a
1050 Vaseline wall across the dish and separately superfused. Gly^1-SIFamide (5 μM) was
1051 bath-applied selectively to the posterior compartment containing the STG. ***B*,** Schematic
1052 of the pyloric and gastric mill connectome. Resistor symbols indicate electrical coupling,
1053 diode symbols indicate rectification of electrical coupling, and ball and stick symbols
1054 indicate chemical inhibition. Colors indicate neurons that participate in the Gly^1-
1055 SIFamide rhythm and are discussed in this study. ***C*,** Representative
1056 electrophysiological traces of the pyloric (*pdn*, *mvn, lpgn*) and gastric mill (*mvn, dgn* and
1057 *lgn*) networks in an example experiment in Saline:Intact STNS (**Ci**), Saline:*ions/sons* cut
1058 (**Cii**) and bath-applied Gly^1-SIFamide (5 μM) (**Ciii**) conditions. The instantaneous pyloric
1059 cycle period is plotted at the top of each set of traces. All conditions are from the same
1060 experiment. ***D*,** The coefficient of variation (CV) of the pyloric cycle period is plotted for
1061 three experimental conditions: 1) in saline prior to isolation of the STG network
1062 (Saline:Intact STNS, n = 19), 2) in saline with *ions/son*s cut to isolate the STG network
1063 from descending modulatory inputs (Saline:*ion*s/*son*s cut, n = 12) and 3) during 5 μM
1064 Gly^1-SIFamide bath application (SIFamide, n = 19). Each dot represents individual

1065 experiments and lines connecting across the experimental conditions depict data points
1066 from the same preparation. The different n value for *ion*s/*son*s cut is due to the lack of a
1067 pyloric rhythm in seven preparations in this condition. In the absence of modulatory
1068 inputs, the pyloric rhythm sometimes shuts off (Zhang et al., 2009; Hamood et al., 2015;
1069 Hamood and Marder, 2015). ***$p < 0.001$, One Way RM ANOVA, Holm-sidak *post hoc*.
1070 Neurons: AB, anterior burster; AM, anterior median; DG, dorsal gastric; GM, gastric mill;
1071 IC, inferior cardiac; Int1, Interneuron 1; LG, lateral gastric; LP, lateral pyloric; LPG,
1072 lateral posterior gastric; MG, medial gastric; PD, pyloric dilator; PY, pyloric; VD,
1073 ventricular dilator. Nerves: *dgn*, dorsal gastric nerve; *ion*, inferior oesophageal nerve;
1074 *lgn*, lateral gastric nerve; *lpgn*, lateral posterior gastric nerve; *lvn*, lateral ventricular
1075 nerve; *mvn*, median ventricular nerve; *pdn*, pyloric dilator nerve; *son*, superior
1076 oesophageal nerve; *stn*, stomatogastric nerve.

1077

1078 **Figure 2. Pyloric cycle periods occurred at three different levels during the Gly^1-**
1079 **SIFamide gastric mill rhythm**. ***A*,** The pyloric rhythm occurs with a shorter cycle period
1080 during LPG activity (blue box), with a longer cycle period during LG:IC activity (pink box)
1081 and an intermediate level in the absence of any gastric mill-timed bursting (SIFbaseline;
1082 grey box). Representative traces show an example rhythm during Gly^1-SIFamide bath
1083 application, with instantaneous pyloric cycle period plotted at the top. Dotted line across
1084 instantaneous cycle period plot indicates SIFbaseline cycle period. ***B*,** The average
1085 pyloric cycle period is plotted for no gastric mill neuron activity (SIFbaseline; grey box)
1086 and during activity of each combination of 1, 2, 3, and 4 gastric mill neurons (n = 19).
1087 Each dot represents the average pyloric cycle period during that particular neuron

1088 activity across a 20 min analysis window during Gly[1]-SIFamide steady state in a single
1089 experiment. Black bars indicate the mean pyloric cycle period across all experiments
1090 during that neuronal activity. Numbers at the bottom of the graph depict the total
1091 number of pyloric cycles contributing to the averages for that neuronal activity. Dotted
1092 line represents average pyloric cycle period during SIFbaseline. Blue box highlights
1093 neuronal activity combinations that include LPG, pink box highlights combinations that
1094 include IC, and purple boxes highlight neuronal activity that include both LPG and IC.

1095

1096 **Figure 3. IC or LG hyperpolarization eliminated longer cycle periods and**
1097 **decreased pyloric cycle period variability.** ***A***, Extracellular and intracellular
1098 recordings monitor the pyloric rhythm (*pdn*) and gastric mill-timed bursting in the IC and
1099 LG neurons in control (Pre; ***Ai***, ***Bi***; Top), during IC (***Aii***) or LG (***Bii***) hyperpolarization,
1100 and after hyperpolarization (Post; ***Aiii***, ***Biii***), all during Gly[1]-SIFamide bath application. A
1101 and B are from different experiments. Pyloric cycle period on top of the extracellular *pdn*
1102 recording plots the instantaneous pyloric cycle period during each condition. Note the
1103 absence of longer pyloric cycle periods during both LG and IC hyperpolarization (pink
1104 boxes indicate LG:IC activity, grey box indicates LG activity without an IC gastric mill
1105 burst (Ai). IC gastric mill bursts are identified by brackets above the IC recordings.
1106 Downward filled arrowheads indicate hyperpolarizing current injection (Aii and Bii).
1107 Downward white arrowheads above instantaneous pyloric cycle period indicate the
1108 SIFbaseline cycle period (dashed line).

1109

1110 **Figure 4. IC hyperpolarization decreased pyloric cycle period variability without**
1111 **altering LG activity.** ***A***, The average CV of pyloric cycle period across 200 sec
1112 windows is plotted for IC (***Ai***, n = 6), LG (***Aii***, n = 4), DG (***Aiii***, n = 4) or all three neurons
1113 (***Aiv***, n = 6) before (Pre), during (Hype) and after (Post) hyperpolarization. ***B***, The
1114 number of IC gastric mill bursts (burst duration > 0.45 s) occurring before (Pre), during
1115 (Hype) and after (Post) LG hyperpolarization is plotted (n = 4). ***C***, LG activity parameters
1116 including burst duration (***Ci***), firing frequency (***Cii***) and number of spikes per burst (***Civ***)
1117 before (Pre), during (Hype) and after (Post) IC hyperpolarization are plotted (n = 6). For
1118 all graphs, data points represent individual experiments connected by lines across
1119 conditions. Grey bars indicate the average across experiments. *p < 0.05, One Way RM
1120 ANOVA, Holm-sidak *post hoc* test.

1121

1122 **Figure 5. LPG photoinactivation decreased pyloric cycle period variability in Gly^1-**
1123 **SIFamide**. ***Ai,*** In control Gly^1-SIFamide with LPG neurons intact, there are shorter cycle
1124 periods during LPG gastric mill-timed bursts (blue box), compared to SIFbaseline
1125 (dashed line) and longer cycle periods during IC activity (pink box). ***Aii***, After both LPG
1126 neurons were photoinactivated (see Methods), pyloric cycle period variability appeared
1127 lower. Pink box highlights an IC gastric mill burst (group of pyloric-timed bursts > 0.45 s
1128 duration). The small units in the *lpgn* recording are PY neurons. ***B***, The pyloric cycle
1129 period coefficient of variation (CV) is plotted for a 20 min window of steady state activity
1130 in the LPG:Intact (blue dots) and LPG:Kill (black dots) conditions (n = 9). Each pair of
1131 dots plus their connecting lines represents a single preparation. Grey bars indicate the
1132 average CV across experiments in each condition. ***p < 0.001, paired t-test. ***C***,

1133 Overlaid histograms (bin size: 3 ms) of all pyloric cycle periods across 20 min windows
1134 during steady state Gly^1-SIFamide application in the LPG:Intact (blue) and LPG:Kill
1135 (grey) conditions (n = 9). Each individual cycle period was normalized to the average
1136 SIFbaseline of the same preparation. Bin count of each condition was normalized to the
1137 peak count of that condition to facilitate comparison of histograms. Brackets on top of
1138 histogram indicate, faster pyloric frequency (shorter pyloric cycle periods), SIFbaseline
1139 (arrow) and slower pyloric frequency (longer pyloric cycle periods).

1140

1141 **Figure 6. IC firing frequency was not affected by LPG photoinactivation. *A***,
1142 Representative traces illustrate differences in IC gastric mill-timed activity (brackets on
1143 top of *mvn* recording) before (***Ai***, LPG:Intact) and after (***Aii***, LPG:Kill) photoinactivation
1144 of the two LPG neurons. Pyloric-timed IC bursts within each IC gastric mill burst were
1145 identified if there was a gap between IC action potentials that coincided with a PD
1146 neuron burst (brackets below *mvn* recording). ***B***, Neuronal activity parameters for IC
1147 gastric mill-timed bursts across 20 min windows during steady state Gly^1-SIFamide bath
1148 application are plotted, including number of bursts (***Bi***), burst duration (***Bii***), number of
1149 spikes/burst (***Biii***), and firing frequency (***Biv***). ***C***, Neuronal activity for IC pyloric-timed
1150 bursts within each gastric mill-timed burst is plotted, including number of bursts (***Ci***)
1151 burst duration (***Cii***), number of spikes/burst (***Ciii***), and firing frequency (***Civ***). Blue dots
1152 indicate LPG:Intact condition and black dots indicate LPG:Kill condition. All dots
1153 represent average activity parameter per experiment with lines connecting the two
1154 conditions in each experiment. Grey bars indicate averages across experiments. *$p <$
1155 0.05, paired t-test.

1156

1157 **Figure 7. The same IC firing frequency did not alter pyloric cycle period in the**
1158 **absence of LPG neurons.** Instantaneous pyloric cycle period is plotted against IC firing
1159 frequency in the LPG:Intact (blue dots) and LPG:Kill (grey dots) during 20 min windows.
1160 Each graph plots the data from a single experiment and each dot represents the
1161 instantaneous pyloric cycle period and the IC firing frequency within its pyloric-timed
1162 burst during the same pyloric cycle. Only cycle periods overlapping with IC gastric mill
1163 bursts (IC bursts > 0.45 s; see Fig. 6) are plotted.

1164

1165 **Figure 8. Biphasic regulation of the pyloric cycle during the Gly^{1}-SIFamide-**
1166 **elicited gastric mill rhythm occurs via rectifying electrical coupling between the**
1167 **LPG neurons and the other pyloric pacemaker ensemble neurons.** Slow gastric mill
1168 bursting in LPG allows sufficient current though the rectifying electrical synapses (diode
1169 symbols) to the AB and PD neurons to increase the frequency of the pyloric rhythm. IC
1170 gastric mill bursting is necessary for rhythmic slowing of the pyloric rhythm. However,
1171 this inhibition appears to act primarily via chemical synaptic inhibition of the LPG neuron
1172 (thick black stick/ball), with a much weaker contribution via chemical inhibition of the AB
1173 and/or PD neuron (thin dotted lines). Triphasic pyloric cycle period durations are
1174 depicted below with schematized AB/PD activity during SIFbaseline (grey), speeding
1175 due to LPG gastric mill-timed slow bursting (blue) and slowing caused by IC gastric mill
1176 bursting (pink).

1177

1178 Table 1. Pyloric cycle period CV in saline (intact STNS or with *ion*s/*son*s transected) and during
1179 bath application of Gly[1]-SIFamide (5 μM).

Pyloric Cycle Period CV Mean ± SEM				p-value		
Saline:Intact STNS (n = 19)	Saline:*ion*/*son* cut (n = 12)	Gly[1]-SIFamide (n = 19)	F (df)	Saline:Intact STNS vs SIFamide	Saline:*ion*/*son* cut vs SIFamide	Saline:Intact STNS vs Saline:*ion*/*son* cut
0.03 ± 0.002	0.08 ± 0.01	0.29 ± 0.04	30.09 (18,2)	<0.001	<0.001	0.182

1180 One-way repeated measures ANOVA, Holm-Sidak *post hoc*; CV, coefficient of variation; df,
1181 degrees of freedom

1182

1183 Table 2. Statistical analysis of active gastric mill neuron contributions to pyloric cycle period
1184 variability during Gly[1]-SIFamide (5 μM) application.

Model Complexity		$X^{2(a,b)}$, df t^{c}, df	p-value
4-factor interaction term removed		0.0612[a], 1	0.8047
All 3-factor interaction terms removed		2.9444[b], 4	0.5672
Final Model:		1.019[b], 5	0.961
Includes LPG, LG, IC, LPG:IC, LG:IC		4.015[a], 10	0.946
Post hoc comparisons of significant 2-factor interactions in final model	LG:IC Present	-3.30[c], 240	0.011
	LG:IC Absent	0.84[c], 239	0.40
	IC:LG Present	-7.15[c], 238	<0.0001
	IC:LG Absent	-1.99[c], 241	0.048
	LPG:IC Present	-6.35[c], 238	<0.0001
	LPG:IC Absent	-3.57[c], 238	0.0004
	IC:LPG Present	-2.69[c], 239	0.008
	LPG:IC Absent	-6.23[c], 238	<0.0001

4-factor within-subjects mixed model ANOVA with iterative elimination of non-significant higher-order interactions. Models were compared to full model[a] or previous level of complexity[b] using a likelihood ratio test. [C]*post hoc* comparisons of estimated marginal means.

1206 Table 3. Pyloric cycle period CV and IC and LG burst parameters in Gly[1]-SIFamide (5 μM)
1207 before, during, and after hyperpolarization of gastric mill neurons.

Manipulation	Parameter	Mean ± SEM			F (df)	p-value		
		Pre	Hype	Post		Pre vs Hype	Hype vs Post	Pre vs Post
Hype IC (n = 6)	Pyloric Cycle Period CV	0.30± 0.06	0.09± 0.02	0.25± 0.07	7.43 (5,2)	0.01	0.04	0.39
Hype LG (n = 4)		0.28± 0.09	0.06± 0.02	0.17±4 0.06	6.09 (3,2)	0.04	0.15	0.22
Hype DG (n = 4)		0.21± 0.05	0.19± 0.06	0.17± 0.04	1.18 (3,2)	ns	ns	ns
Hype IC/LG/DG (n = 6)		0.27± 0.066	0.10± 0.05	0.26± 0.06	9.13 (5,2)	0.01	0.01	0.86
Hype LG (n = 4)	# of IC Bursts	12.75± 1.80	1.50± 1.50	12.75± 1.44	22.75 (3,2)	0.003	0.002	1
Hype IC (n = 6)	LG Burst Duration (s)	4.63± 1.01	5.08± 0.95	6.51± 1.25	1.52 (5,2)	ns	ns	ns
	LG # Spikes/Burst	15.34± 5.16	16.50± 5.54	21.79± 5.73	0.49 (5,2)	ns	ns	ns
	LG Firing Freq. (Hz)	2.90± 0.39	2.91± 0.49	3.07± 0.46	0.04 (5,2)	ns	ns	ns

1208 Pre, before hyperpolarization of neuron(s); Hype, during hyperpolarization of neuron(s); Post,
1209 after hyperpolarization of neuron(s); CV, coefficient of variation; df, degrees of freedom; ns, p*ost*
1210 *hoc* not performed when $p > 0.05$; One-way repeated measures ANOVA, Holm-Sidak *post hoc*

1211

1212 Table 4. IC gastric mill and pyloric burst parameters during LPG Intact and LPG

1213 photoinactivated (Killed) conditions in Gly[1]-SIFamide (5 μM).

		Mean ± SEM			
		LPG Intact	LPG Killed	*t, df*	*p-value*
IC Gastric mill bursts (n = 9)	# bursts	68.89 ± 9.50	68.33 ± 9.98	0.12, 8	0.91
	Burst Duration (s)	5.08 ± 0.65	4.33 ± 0.34	1.48, 8	0.18
	# Spikes/Burst	64.59 ± 9.53	55.02 ± 7.04	1.71, 8	0.13
	Firing Freq. (Hz)	12.96 ± 1.02	12.47 ± 0.86	0.93, 8	0.37
IC, pyloric bursts (n = 9)	# bursts	249.56 ± 35.09	262.22 ± 35.02	-0.78, 8	0.46
	Burst Duration (s)	1.31 ± 0.14	1.01 ± 0.20	2.00, 8	0.08
	# Spikes/Burst	19.02 ± 2.16	13.37 ± 2.03	2.81, 8	0.02
	Firing Freq. (Hz)	14.14 ± 1.61	13.83 ± 1.72	0.65, 8	0.53

1214 During Gly[1]-SIFamide application; paired t-test

1215

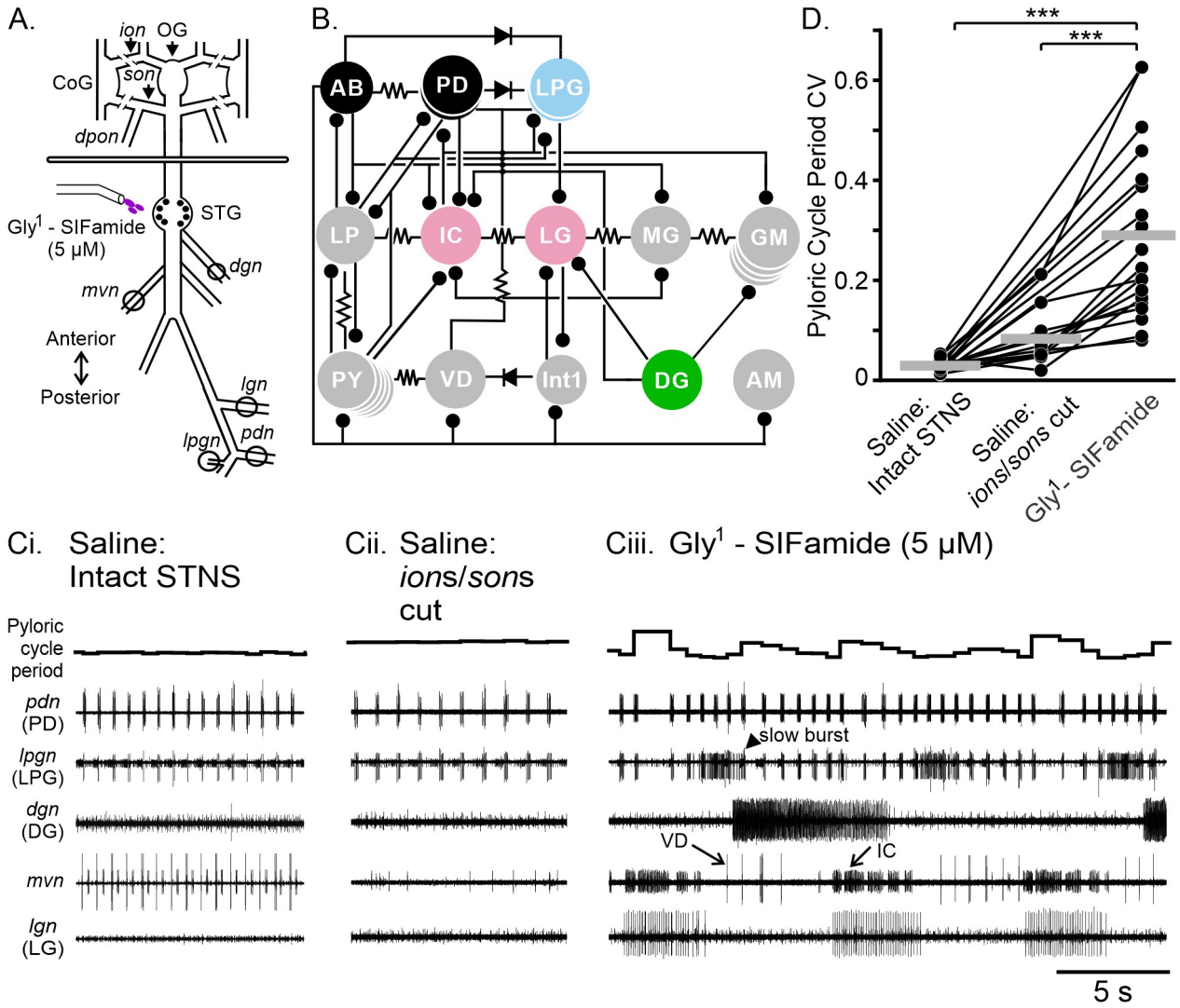

Figure 1
Gnanabharathi, Fahoum & Blitz

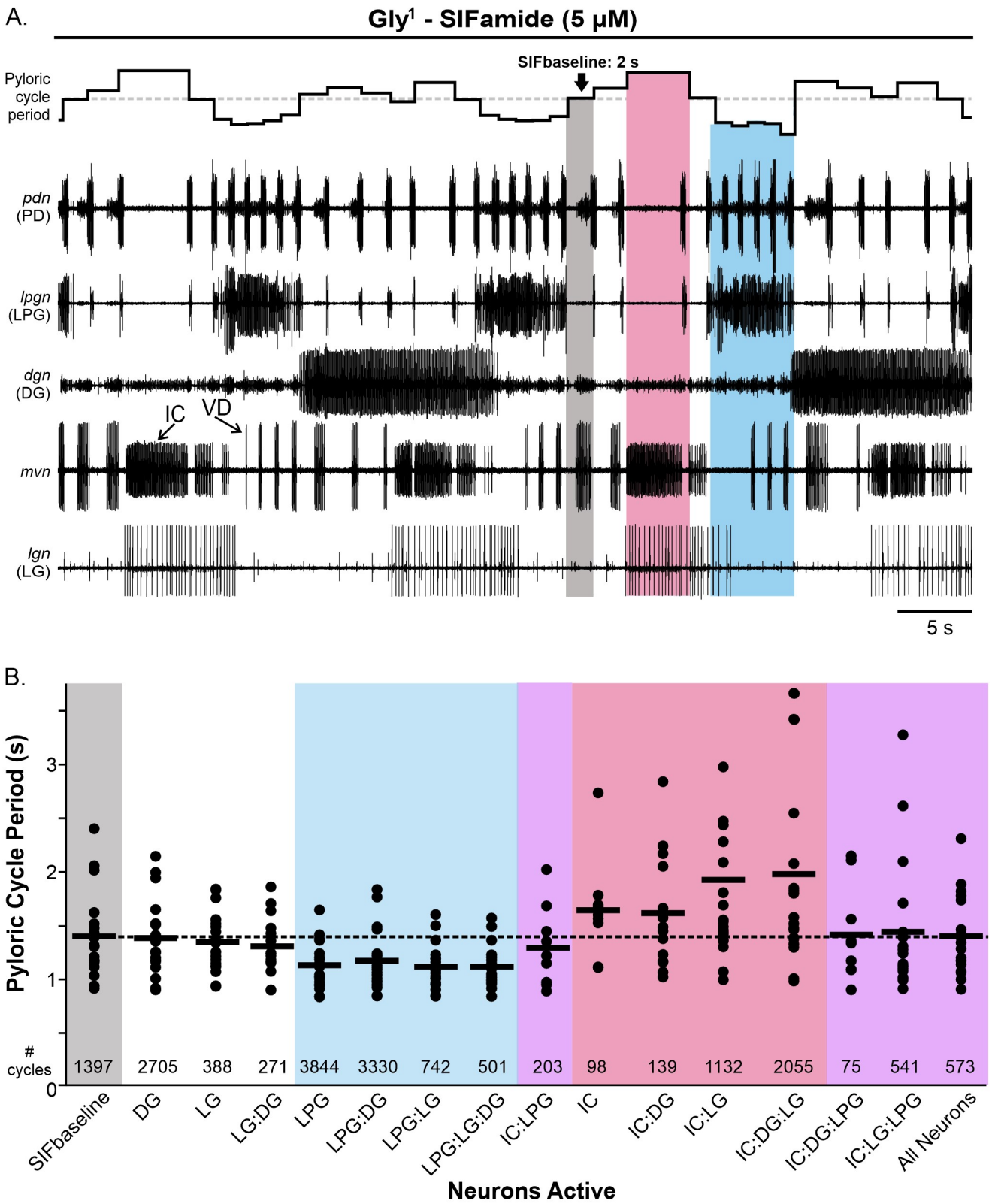

Figure 2
Gnanabharathi, Fahoum & Blitz

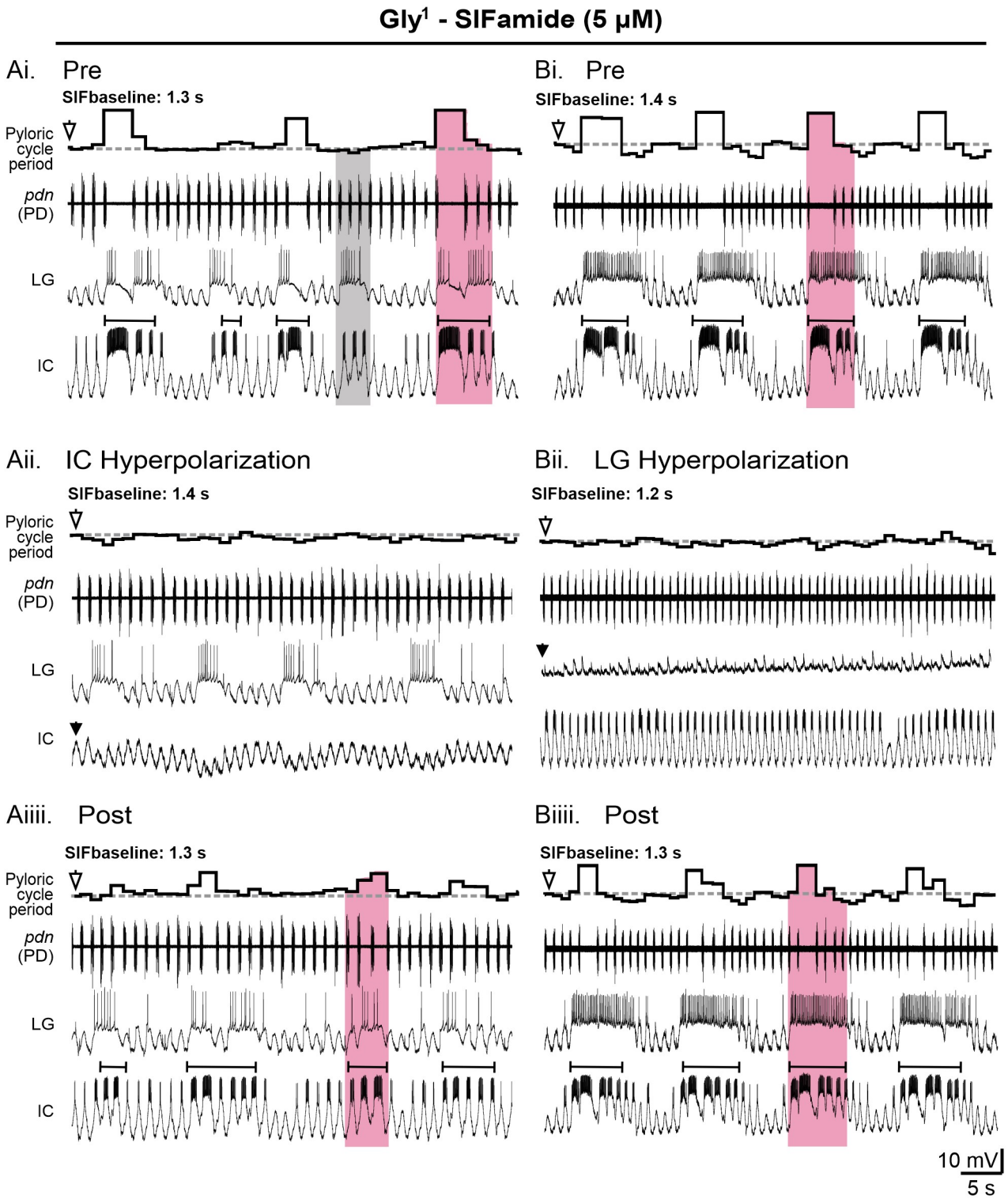

Figure 3
Gnanabharathi, Fahoum & Blitz

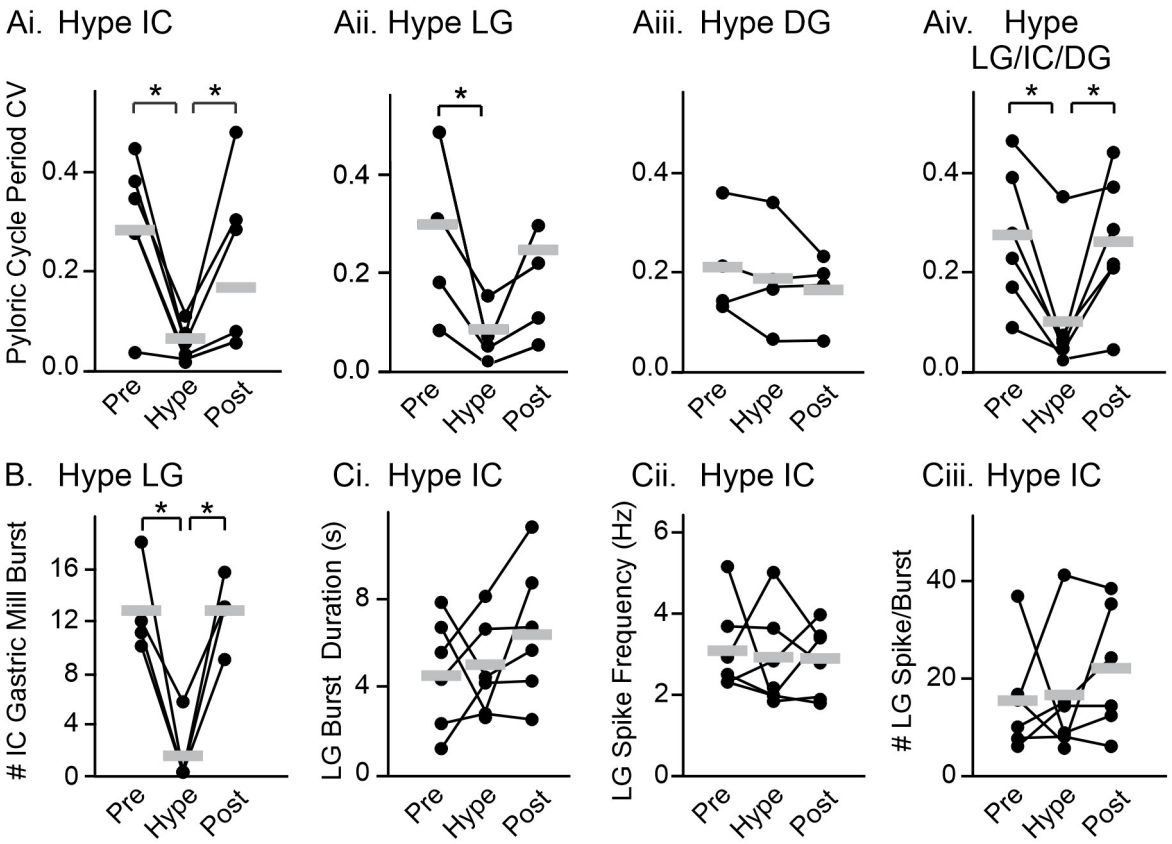

Figure 4
Gnanabharathi, Fahoum & Blitz

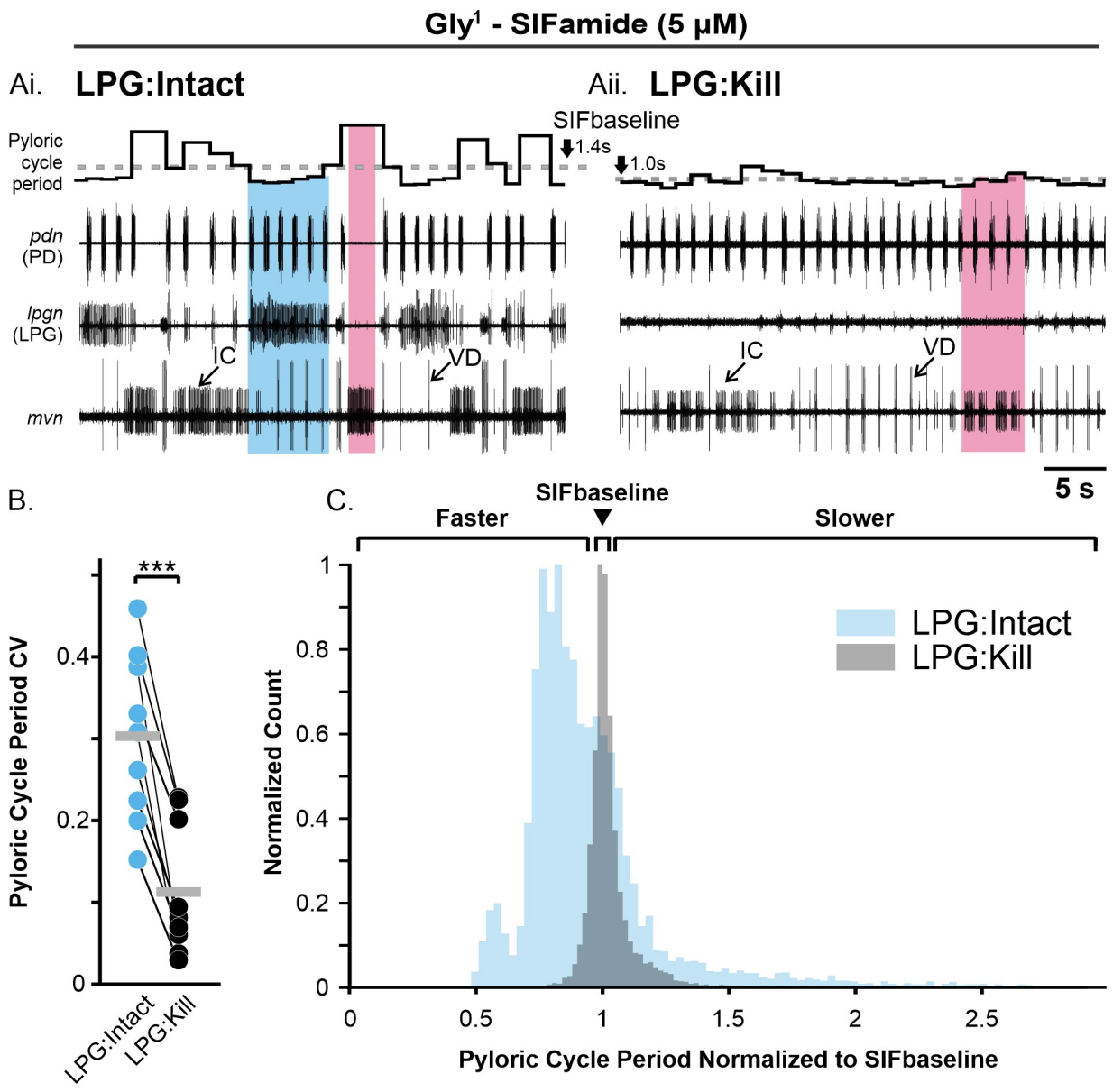

Figure 5
Gnanabharathi, Fahoum & Blitz

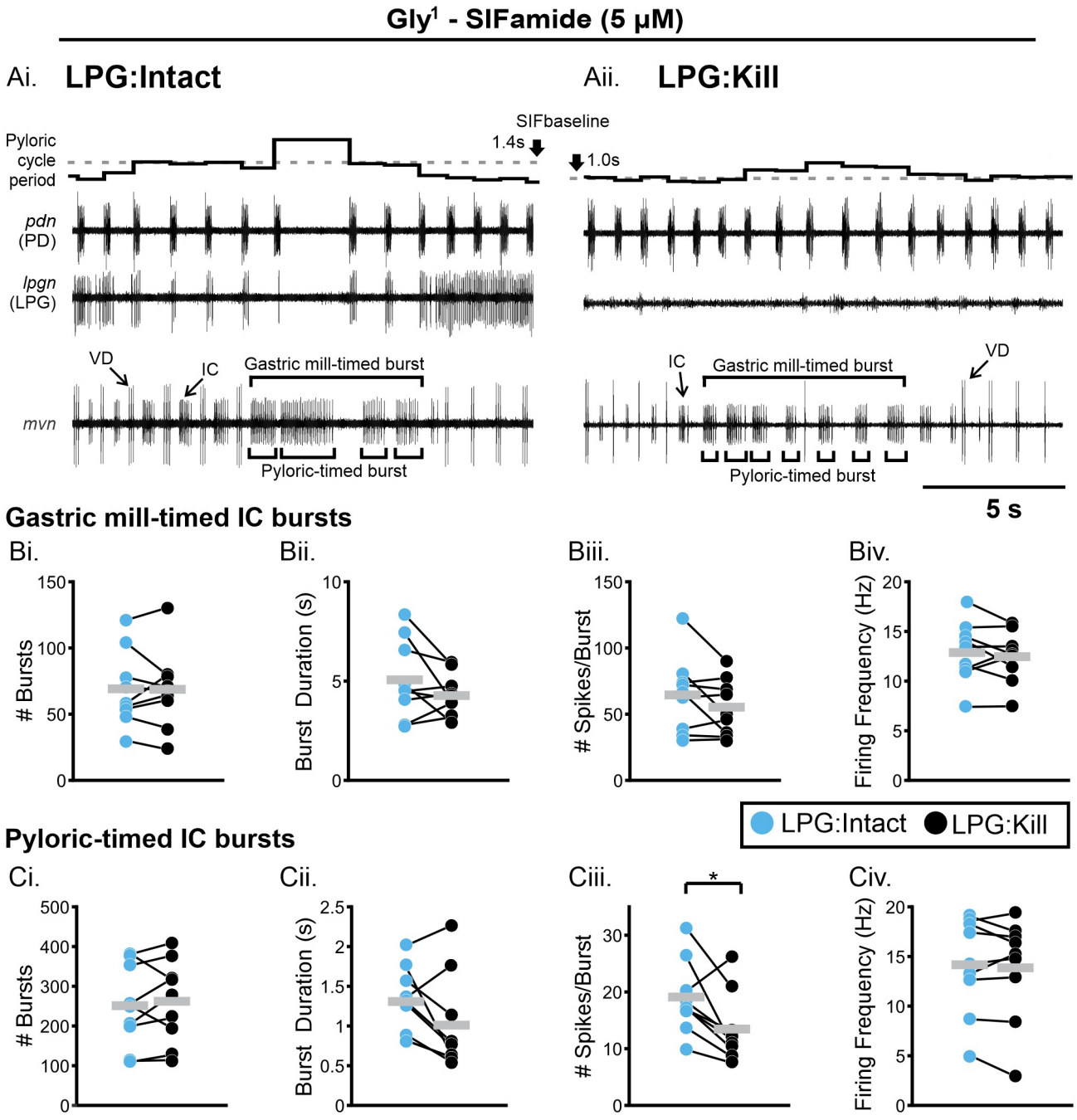

Figure 6
Gnanabharathi, Fahoum & Blitz

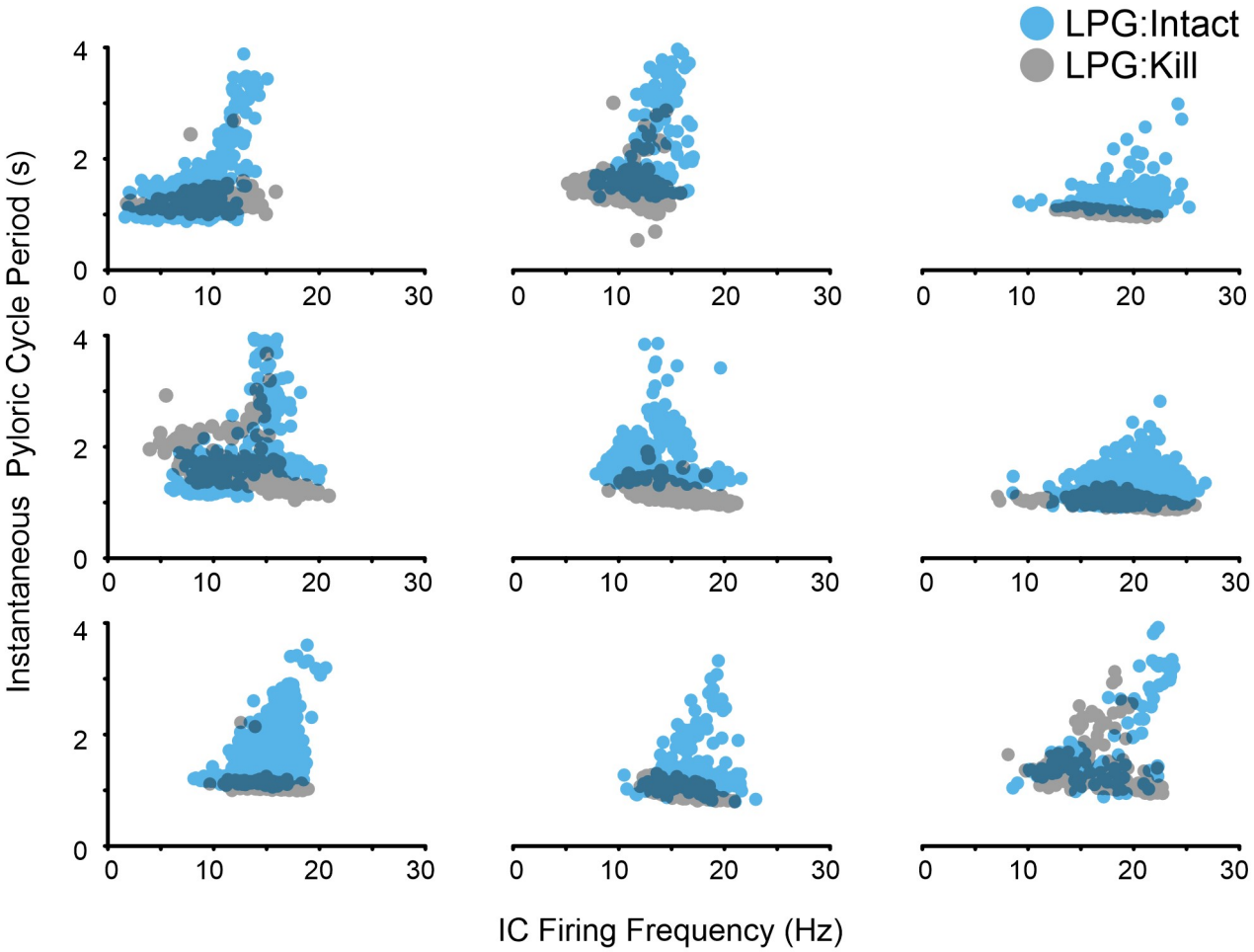

Figure 7
Gnanabharathi, Fahoum & Blitz

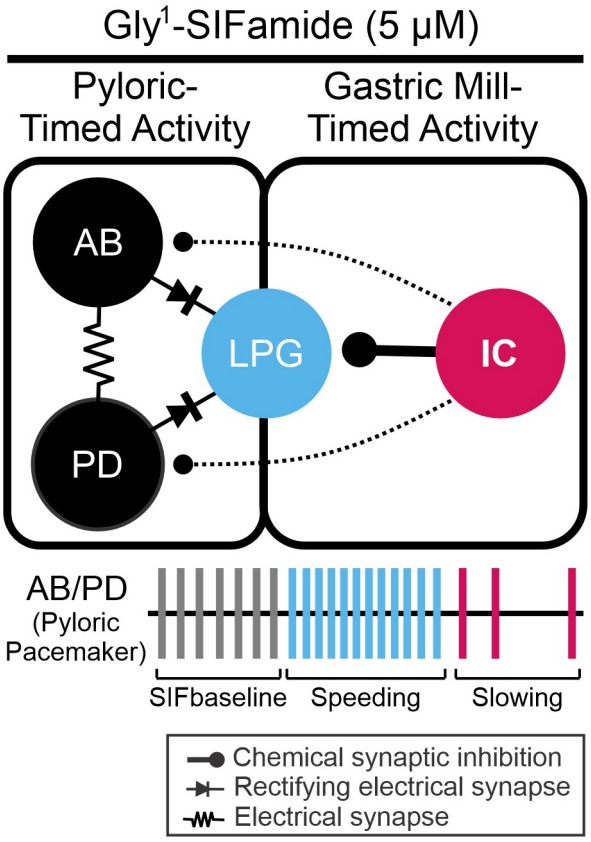

Figure 8
Gnanabharathi, Fahoum & Blitz